REPORT NO. 3477
COPY NO. 15

PHOTOVISCOUS TECHNIQUE DEVELOPMENT

Volume I - Theory and Experiments

THE Bendix CORPORATION

RESEARCH LABORATORIES DIVISION

SOUTHFIELD, MICHIGAN

Report No. 3477

PHOTOVISCOUS TECHNIQUE DEVELOPMENT

Volume I - Theory and Experiments

15 June 1966

CONTRACT NAS 8-5407, PHASE III

Submitted to

National Aeronautics and Space Administration
George C. Marshall Space Flight Center
Huntsville, Alabama 35812

By

The Bendix Corporation
Research Laboratories Division
Southfield, Michigan 48076

Prepared by: F. M. Faubert

F. M. Faubert, Engineer
Applied Mechanics Department
Energy Conversion and Dynamic Controls Laboratory

Approved by: B. R. Teitelbaum

B. R. Teitelbaum, Head
Applied Mechanics Department
Energy Conversion and Dynamic Controls Laboratory

Approved by:

L. B. Taplin, Manager
Energy Conversion and Dynamic Controls Laboratory

ABSTRACT

This project concerned the application of photoviscosity to experimental investigations of flow fields in fluid devices. Milling Yellow dye solutions were used in the experiments. The analytical relationships between the optical phenomena and two-dimensional flow kinematics were summarized and presented. Test equipment was developed for applying the photoviscous technique to a variety of transparent models simply and conveniently. The use of a rectangular channel model, integral with the fluid circulation system, was demonstrated as a calibration device for obtaining the optic response of the photoviscous liquid.

The majority of the quantitative testing was performed using a vortex model with no tangential flow. A comparison was made of the radial distribution of the fluid deformation rate as determined (a) analytically, and (b) by photoviscous experiments. The agreement was poor, which is attributed to the low aspect ratio (depth-to-width ratio) of the model. The comparison demonstrated (a) the importance of the aspect ratio criterion, if quantitative determination of a flow field is of interest, and (b) the need for studying the three-dimensional stress-optic law for Milling Yellow dye solution to extend the utility of the technique.

The combination of photoviscosity with high-speed motion picture photography was found to be a potentially valuable technique for studying the internal dynamic response times in fluid flow models. Several kinds of qualitative information obtainable, using photoviscosity, are described. Recommendations are made for adding rheological calibration to optical calibration of the working fluid to refine the photoviscous technique.

VOLUME I

TABLE OF CONTENTS

VOLUME I

LIST OF ILLUSTRATIONS

FOREWORD

This report was prepared by the Research Laboratories Division of the Bendix Corporation as part of the research and study performed under Contract NAS 8-5407, Phase III, "Development of a Photoviscous Technique for Fluid Flow Studies," for the George C. Marshall Space Flight Center, National Aeronautics and Space Administration.

The project engineer for the Marshall Space Flight Center was Mr. Jerry A. Peoples.

The technical work performed at the Bendix Research Laboratories Division was the responsibility of Mr. F. M. Faubert. The project work was initiated by Mr. B. S. Fichter, who made many contributions throughout the project duration. The work was performed in the Applied Mechanics Department, headed by Mr. B. R. Teitelbaum.

The report is published in two volumes. Volume I - Theory and Experiments treats the analytical foundation of the photoviscous technique and describes the results of experiments performed during the project. Volume II - Photoviscous Test Stand describes the equipment developed during the project, and gives operating and maintenance information.

SECTION 1

INTRODUCTION

This report presents a summary of the work performed by Bendix Research Laboratories Division under Phase III, "Development of a Photoviscous Technique for Fluid Flow Studies," Contract NAS8-5407 from the George C. Marshall Space Flight Center, National Aeronautics and Space Administration. The effort was directed toward the quantitative use of photoviscosity for studying the flow fields in fluid components. In this introduction the photoviscous flow visualization principles will be described briefly. More detailed technical discussion and descriptions of the equipment and procedures developed are given in subsequent sections.

In recent years, the photoelastic technique has proved to be a powerful tool in the field of experimental stress analysis. The technique is based on the phenomenon of temporary double refraction which occurs in certain substances when subjected to a system of shear stresses. When such a substance, while in a stressed condition, is placed between two polarizing plates and viewed by transmitted light, visible fringe patterns are produced. These patterns are related to the material properties and dimensions of the model, and to the stress in the model. In general, the technique has been used primarily for two-dimensional problems, but special techniques have been found which permit analysis of three-dimensional systems. An extensive treatment on photoelastic theory and practice has been presented by Frocht.[5]

An analogous phenomena was reported in the area of liquids in 1873 by J. C. Maxwell,[14] when he reported the doubly refracting properties in Canada Balsam. Since that time, many extensive investigations have been performed on a wide range of liquids to determine the relative strengths of this doubly refracting characteristic.

This phenomenon in liquids has been referred to as streaming birefringence, streaming double refraction, flow double refraction and photoviscosity. The terms are used interchangeably in the literature.

The extensive investigations performed since Maxwell's time have shown that a large number of liquids exhibit some degree of

birefringence. In most liquids, however, the amount is too small to develop even the first fringe at velocity gradients of interest in normal hydraulic research.

Those liquids exhibiting a low optical sensitivity (birefringence) require point-by-point evaluation of the amount of birefringence by optical compensation techniques. Liquids with a low optical sensitivity usually display linear birefringent characteristics, and the fluid behavior is Newtonian. (The viscosity is independent of the shear stress existing in the fluids.)

Liquids with a high optical sensitivity can be categorized as colloidal solutions (in contrast to the fluids exhibiting low optical sensitivity, which are pure liquids) such as bentonite, vanadium pentoxide, etc. These solutions exhibit birefringent characteristics greater than the pure liquids by a factor of about 10^8. The characteristics of the solution include non-Newtonian flow behavior (viscosity a function of shear stress) in addition to nonlinear birefringent characteristics.

A birefringent liquid produces a field of visible interference patterns when subjected to shear stresses due to flow, placed between polarizing plates, and illuminated by monochromatic light. These patterns are alternately light and dark bands in the flow field. The patterns are stationary in laminar flows and exhibit a random eddying motion in turbulent flows. The dark bands formed are of two types, referred to as isochromatics and isoclinics. The isochromatics are related to the magnitude of the maximum rate of deformation in the flow, while the isoclinics are related to the direction of this rate of deformation. If the polarized light is plane, both the isoclinics and the isochromatics are visible; if circularly polarized light is used, only the isochromatics appear.

When white instead of monochromatic light is used, color bands are produced, rather than dark and light bands. Generally, the color bands lack the detailed structure of corresponding dark and light monochromatic bands.

In 1953, Peebles, Barber, and Jury[15] reported finding a fluid which was well-suited for quantitative flow analysis for steady two-dimensional flow. This fluid is an aqueous suspension of a commercially-available dye, called Milling Yellow NGS*. The

*Trade name of commercial dyestuff produced by Allied Chemical and Dye Company.

suspension was shown to be very stable over long periods of time, and exhibited excellent birefringent characteristics for concentrations as low as 1.2 percent by weight. In addition, its viscosity is similar to that of MIL-O-5606 hydraulic oil, making it well-suited for hydraulic test work.

The purpose of the present investigation was to determine the applicability of the doubly-refracting Milling Yellow suspension for analyzing the fluid flow phenomena occurring in two-dimensional fluid state devices. It was decided that the objectives of this project should be twofold. The first objective was to demonstrate that a rectangular channel of high aspect ratio (depth-to-width ratio) could be used to obtain the birefringent characteristics of a fluid of any concentration and at any temperature, as a function of the strain rate. The second objective was to demonstrate that the strain rate and velocity distributions obtained for an actual fluid state test model by the photoviscous technique would correlate closely with the distributions predicted by purely analytical considerations.

SECTION 2

REVIEW OF PREVIOUS WORK

A large number of investigators have concerned themselves with the molecular physics aspects of these birefringent liquids. There have been some who have attempted to utilize the birefringent characteristics for obtaining qualitative and quantitative conclusions concerning fluid flow problems.

As early as 1923, Humphrey[9] made qualitative studies on the transition phenomenon from laminar to turbulent flow, utilizing a colloidal solution of vanadium pentoxide in water. Further qualitative studies were made along the same line by Leaf[12] in 1945, using bentonite sols to obtain information on locomotive firebox design. Binnie[2] and Lindgren[13] also studied the laminar-to-turbulent transition phenomenon, using benzopurpurin and bentonite, respectively.

The first attempts at quantitative work were made by Alcock and Sadron[1] in 1936. They used sesame oil with a high viscosity and a low optical sensitivity. It was stable over long periods,however, which was in sharp contrast to colloids used previously.

From 1940-1942, Hauser and Dewey[4][6][7] performed very extensive qualitative and quantitative studies of two-dimensional velocity profiles using bentonite sols. They studied such complex shapes as automobile bodies, and used both white and monochromatic light sources for their studies. The quantitative results from these studies were extremely questionable, since they had assumed that the isoclinics were related to the streamline directions rather than the shear direction. A further weakening assumption was that the isochromatic fringes were determined by the velocity gradient normal to the streamlines, rather than the total shearing stress in the liquid.

A careful analytical study of flow double refraction was made by Rosenberg[20] in 1952. He showed that the direction of maximum shear stress and the direction of the streamlines were coincident only for flow with parallel streamlines. He also suggested a method for analyzing a general two-dimensional flow problem from the isochromatic

bands appearing in the field. He included a detailed bibliography and summarized the non-linearities involved in the utilization of colloidal solutions in flow visualization.

As was indicated previously, the application of colloidal solutions of Milling Yellow dye to study velocity profiles in two-dimensional flow systems was reported by Peebles, Garber, and Jury in 1953. The rheologic properties of this organic dye were later published by Peebles, Prados, and Honeycutt[17].

Quantitative techniques have been demonstrated by Prados[18] for flow between parallel walls, converging and diverging channels, and flows about a cylindrical obstacle in a rectangular channel. Prados utilized Milling Yellow dye solutions to produce the fringe patterns. Sample calculations were included for each flow analysis. All studies used flow models having a depth-to-width ratio of at least 5.

SECTION 3

THEORY

The use of a doubly refracting suspension in investigating a two-dimensional flow field requires a familiarity with certain optical equipment, phenomena and terms, which will be discussed here.

3.1 POLARIZED LIGHT

Light can be viewed as vibrations of an electric field vector in planes perpendicular to the light propagation direction. Ordinary white light consists of vibrations of all ranges of amplitudes, wavelengths, and orientations. In most birefringent studies, polarized light is used. Polarized light can be classified into three categories, being plane polarized, elliptically polarized, and circularly polarized. Plane polarized light consists of vibrations which all have the same orientation; that is, all lying in a single plane through the propagation direction line. Elliptically polarized light is characterized by two sets of vibrations having mutually perpendicular orientations, being 90 degrees out of phase with each other, and having unequal amplitudes. If the amplitudes are equal, the light is referred to as circularly polarized. The resultant of the two sets of vibrations in circularly polarized light is a single electric field vector, of constant amplitude, which rotates about the line of propagation at the light vibration frequency.

Polarized light is obtained by utilizing the properties of certain optical elements, the most common of which are the Nicol prism and the Polaroid sheet. The polarization of the Nicol prism is based on birefringence and that of the Polaroid sheet is based on dichroism.

In the birefringent material, an entering light ray is resolved into two rays, both plane polarized with their polarization orientations mutually perpendicular. One of the rays follows the law of refraction for ordinary materials, and is called the ordinary ray. The other, called the extraordinary ray, follows a different law of refraction. The speeds of propagation for the two rays in the birefringent material are different also. By the design of the Nicol prism element, the ordinary ray is deviated from the optical path, and the extraordinary ray is transmitted. This ray is plane polarized with a specific orientation corresponding to an axis fixed in the Nicol prism.

In the dichroic polarizers, the entering ray is also resolved into two plane polarized rays. One of these is strongly absorbed by the dichroic material. Thus, the element serves as a filter which passes only light having a specific polarization orientation with respect to an axis fixed in the material. For photoviscous flow visualization, the dichroic Polaroid sheets provide the more economical method of obtaining plane polarized light.

Circularly polarized light is obtained by placing (in the optical path) a quarter-wave plate or layer which the light enters after leaving a plane polarizer. The quarter-wave element is made of birefringent material and its optic axes have a definite orientation with respect to the plane of polarization of the entering light. The quarter-wave element resolves the entering ray into ordinary and extraordinary rays with equal amplitudes and perpendicular polarization orientations. The difference in speeds of the two rays, and a specific thickness of the quarter-wave element, cause the two rays to arrive at the end of the element 90 degrees (or a quarter of a wave length) out of phase. There are then sufficient conditions for the light to be circularly polarized. For a given element thickness, there is only one wavelength of light which will result in true circular polarization. Other wavelengths result in elliptic polarization. In practice, a fair degree of ellipticity can be tolerated in a photoviscous flow visualization apparatus; so exact matching of the quarter-wave element to the light wavelength being used is not critical.

Separate quarter-wave plates are usually employed when Nicol prisms are providing the plane polarized light. When Polaroid sheets are being used, a quarter-wave layer, integrally bonded to a Polaroid sheet, is employed.

If one considers how the various polarizing elements operate on an incident light ray, regardless of the physical phenomena involved, their action can be summarized as follows: A plane polarizer will transmit only the component of the incident light vibration vector which is along the polarizer axis. A quarter-wave element will convert an incident plane-polarized ray into a circularly polarized ray. Conversely, a quarter-wave element will convert an incident circularly polarized into a plane-polarized ray.

3.2 PHOTOVISCOUS FRINGE PRODUCTION

The use of plane-polarized light to measure the amount of birefringence produced by a stressed substance has been thoroughly investigated, and the quantitative features of this phenomenon have been treated by Frocht[5] and Jessop and Harris[11]. If plane-polarized light passes through a birefringent liquid and then through a second polarizer (conventionally called an analyzer) whose polarization axis is at 90 degrees to that of the first polarizer, the vibration of the transmitted light can be described by

$$R = A \sin 2\beta \sin \frac{\delta}{2} \sin \omega t \qquad (3.1)$$

where the symbols are as follows:

- R = resultant light vector leaving the analyzer
- A = amplitude of the light vector leaving the polarizer
- ω = frequency of oscillation of the light vector
- δ = relative retardation between the fast and slow (extraordinary and ordinary) rays.
- t = time
- β = angle between the polarizer axis and the local optic axis of the fluid.

It should be pointed out that the effect of the local shearing stress results in the formation of two mutually-perpendicular optic axes of the fluid. The orientations of these axes are related to the orientation of the maximum rate of deformation in the fluid. It is due to this effect that the fluid becomes birefringent, similar to the materials used for polarizers.

The proof of this relation can be demonstrated by considering the light vector leaving the first polarizer as

$$u = A \cos \omega t \qquad (3.2)$$

where the symbols are defined above.

Referring to Figure 3-1, the components of this vector along the local optic axes of the fluid can be determined to be

$$S' = A \cos\left(\omega t - \frac{\delta}{2}\right) \cos\beta \qquad (3.3a)$$

$$F' = -A \cos\left(\omega t + \frac{\delta}{2}\right) \sin\beta \qquad (3.3b)$$

where S' and F' are the components in the direction of the optic axes for the light ray leaving the fluid. It should be noted here that the relative retardation that occurred in passing through the fluid has been divided between the fast and slow rays.

The components of these rays leaving the analyzer then become

$$S = A \cos\left(\omega t - \frac{\delta}{2}\right) \cos\beta \sin\beta \qquad (3.4a)$$

$$F = -A \cos\left(\omega t + \frac{\delta}{2}\right) \sin\beta \cos\beta. \qquad (3.4b)$$

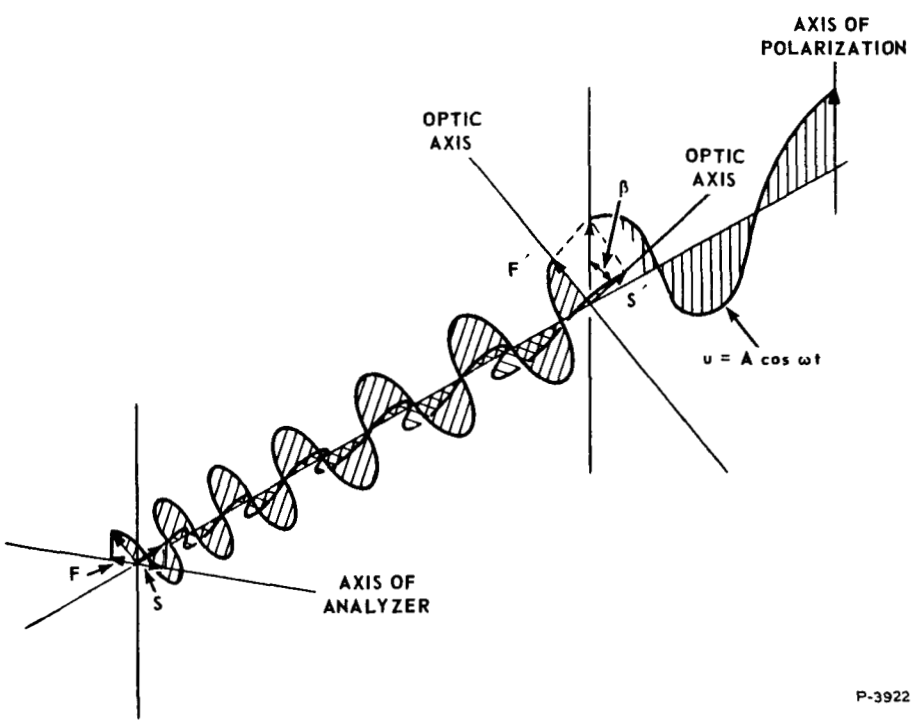

Figure 3-1 - Polarized Light in Birefringent Fluid

The resultant magnitude of these vectors is

$$R = -A \sin\beta \cos\beta \left[\cos\left(\omega t + \frac{\delta}{2}\right) - \cos\left(\omega t - \frac{\delta}{2}\right)\right] \qquad (3.5)$$

By utilizing the trigonometric identities that

$$\sin 2\beta = 2 \sin\beta \cos\beta \qquad (3.6a)$$

and

$$\sin\omega t \sin\frac{\delta}{2} = -\frac{1}{2}\left[\cos\left(\omega t + \frac{\delta}{2}\right) - \cos\left(\omega t - \frac{\delta}{2}\right)\right] \qquad (3.6b)$$

the result obtained is

$$R = A \sin 2\beta \sin\frac{\delta}{2} \sin\omega t \qquad (3.1)$$

as asserted.

Since the intensity of the transmitted light is proportional to the square of its amplitude of vibration, zero intensity occurs only when

$$\beta = N\left(\frac{\pi}{2}\right) \qquad N = 0, 1, 2, ... \qquad (3.7a)$$

$$\delta = 2\pi N \qquad N = 0, 1, 2, ... \qquad (3.7b)$$

Thus, the intensity of the transmitted light is zero when either the direction of the incident polarized ray is along any fluid optic axis, or when the phase difference over the optical path is zero or some multiple of a whole wavelength. The phase difference δ can be expressed as

$$\delta = 2\pi \frac{L}{\lambda}\left|n_e - n_o\right| \qquad (3.8)$$

where

λ = wavelength of the monochromatic light source

L = optical path thickness in the fluid

$n_e - n_o$ = difference between the extraordinary and ordinary indices of refraction

Equation (3.8) can be obtained by considering a side view of a test section, where the light is entering normal to the wall, as shown in Figure 3-2.

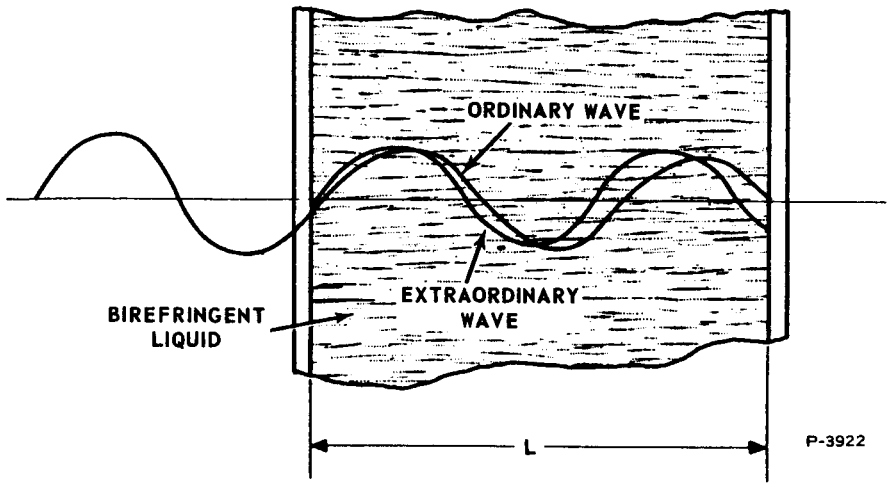

Figure 3-2 - Phase Difference

Because of the doubly refracting properties of the fluid, two rays of waves will be produced, and will travel at different speeds through the liquid. The number of cycles that each wave will undergo in this thickness L is given by

$$C_o = \frac{L}{\lambda_o} \tag{3.9a}$$

$$C_e = \frac{L}{\lambda_e} \tag{3.9b}$$

where

C_e, C_o = number of cycles for the extraordinary and ordinary rays

λ_e, λ_o = wavelength of the extraordinary and ordinary rays in the fluid.

The difference in number of cycles is

$$C_e - C_o = \frac{L}{\lambda_e} - \frac{L}{\lambda_o} \tag{3.10}$$

It must be recalled that both the ordinary and the extraordinary waves are oscillating at the same frequency, and therefore the phase shift is

directly proportional to the relative displacement between the two waves, which in this case is $C_e - C_o$. Therefore, the phase shift, in cycles, is

$$\delta = C_e - C_o = \frac{L}{\lambda_e} - \frac{L}{\lambda_o} \tag{3.11}$$

Multiplying the numerator and denominator of both terms on the right hand side by λ, and multiplying by 2π gives the phase shift in radians.

$$\delta = \frac{2\pi L}{\lambda}\left(\frac{\lambda}{\lambda_e} - \frac{\lambda}{\lambda_o}\right) \tag{3.12}$$

Recalling the definition for index of refraction, we have

$$\frac{\lambda}{\lambda_e} = n_e \tag{3.13a}$$

$$\frac{\lambda}{\lambda_o} = n_o \tag{3.13b}$$

which upon substitution into equation (3.12) gives

$$\delta = \frac{2\pi L}{\lambda}\left|n_e - n_o\right| \tag{3.8}$$

When a model of a fluid device is illuminated by monochromatic plane polarized light, there will be dark bands produced by conditions corresponding to equations (3.7a) and (3.7b). The dark bands produced by condition (3.7a) are called isoclinics, and these bands are loci where one of the local optic axes of the fluid is aligned with the direction of vibration of the polarized incident light. The bands produced by conditions corresponding to(3.7b) are referred to as isochromatics. If plane polarized white light is used rather than monochromatic light, dark bands will occur in the flow field only as a result of condition (3.7a) and for N = 0 in condition (3.7b). This is because white light consists of a continuum of wavelengths, and no single phase difference is obtained which cancels all the light. The isochromatics will appear rather as color fringes, and the relation between the color fringes and the fringe order has been reported by Thurston[21] as follows:

Fringe Order	Color
0	Black
1	Yellow

Fringe Order	Color
2	Red
3	Green
4	Yellow
5	Red
6	Green, etc.

If quarter-wave elements are inserted into the optical path such that one is placed between the polarizer and the test model and the other is placed between the model and the analyzer, circularly-polarized rather than plane-polarized light enters the liquid, and is changed back to plane-polarized light before reaching the analyzer (second polarizer). The vibration vector of the circularly-polarized light is continuously rotating around the propagation direction at the vibration frequency. This continuous rotation eliminates the possibility of dark spaces occurring from a condition predicted by (3.7a), since the entering ray vector has no special orientation with respect to the fluid optic axes. Thus, the use of circularly polarized light eliminates the isoclinics.

3.3 SHEAR-OPTIC RELATIONS

There are two basic theories as to what causes a fluid to be anisotropic, or birefringent. The first is referred to as the viscoelastic theory, and it assumes that birefringence is generated by stretching and orientation of long polymer-like chains. The second theory assumes that the birefringence is generated by the orientation of suspended particles, which are shaped like long rods. An accurate analysis of the motion of such particles in viscous incompressible flow is extremely difficult, due to the complexity of the hydrodynamic equations. In addition, there is the added complication of the Brownian movement effect. This effect results from the interaction of the colloidal solution particles and the molecules of the surrounding medium.

Jeffery[10] obtained the equations of motion for small ellipsoidal particles in which the Brownian movement was neglected. Even with this simplifying assumption, he could obtain a solution only to the equations for the special case of:

$$u = C\,y, \quad v = w = 0$$

where

u = velocity in x direction

v = velocity in y direction

w = velocity in z direction

C = constant

y = geometric coordinate

Jeffery's analysis was extended by Boeder[3] for the same flow conditions, and included the effect of the Brownian movement. He showed that the extinction angle (the angle between the optic axis of the particle and the direction of the maximum deformation rate) and the birefringence were functions of both the intensity of the Brownian movement, and the velocity gradients or the deformation rate. It was found that the extinction angle was 45 degrees at low velocity gradients and decreased with increasing velocity gradient. The dependence of the extinction angle and the birefringence on the deformation rate were in general nonlinear.

The amount of birefringence in a doubly-refracting fluid can be expressed as the difference in indices of refraction between the ordinary and the extraordinary rays, and can be calculated from

$$|n_e - n_o| = \lambda \mu M E_{max} \tag{3.14a}$$

where

μ = fluid viscosity

λ = wavelength of the monochromatic light source

E_{max} = maximum rate of deformation

M = quantity called the Maxwell constant

The equation indicates that for a Newtonian fluid, the ratio

$$\frac{|n_e - n_o|}{E_{max}} = \lambda \mu M \tag{3.14b}$$

is a constant, for a fixed value of λ. However, experimental data have shown that for Milling Yellow dye solution, the relation between $|n_e - n_o|$ and E_{max} is not linear even when the viscosity μ does not vary. Therefore, it has been concluded that the Maxwell's constant is really not a constant,

but rather is a function of the maximum strain rate. This supports the theory that the birefringence of Milling Yellow dye results from the orientation of particles.

The experimental determination of the optical properties of a photoviscous fluid are usually obtained utilizing a device known as a concentric cylinder polariscope, which is shown in Figure 3-3. The fluid to be calibrated is placed in the annular space between the two cylinders in which a known strain rate can be set up in the fluid by causing the outer cylinder to rotate. The magnitude of this strain rate at the center of the annular space can be expressed as

$$E = \frac{\tau_{r\theta}}{\mu} = \frac{8\,\omega\, r_1^2\, r_2^2}{\left(r_1 + r_2\right)^2 \left(r_2^2 - r_1^2\right)} \tag{3.15}$$

where r_1 and r_2 are the inner and outer radii, respectively, and ω is the angular speed by the outer cylinder. Proof of this expression can be obtained quite easily from the Navier-Stokes equations.

The experimental techniques used in obtaining the values of the extinction angle χ and the birefringence as a function of strain rate in the cell has been described in detail by Peebles, Prados and Honeycutt[17]. (The extinction angle χ is defined as the angle formed by the local optic axis and the direction of the maximum rate of deformation.) Basically, the birefringence is obtained by observing the fringes produced as the speed of the outer cylinder is increased, and recording both the fringe order N and the speed of rotation ω when the fringe is exactly at the center of the gap. By utilizing the relation between fringe order and birefringence (obtained by equating (3.7b) and (3.8))given by

$$\left|n_e - n_o\right| = \frac{N\lambda}{L} \tag{3.16}$$

and equation (3.15) for a range of outer cylinder speeds, a plot of birefringence versus strain rate can be obtained for the fluid. Determination of the extinction angle as a function of strain rate is obtained by aligning a set of cross-hairs which are calibrated with respect to the plane of polarization with one of the four dark bands formed in the cell, as shown in Figure 3-4. Four such bands appear in the polariscope in the form of a cross, and are referred to as the "cross of isoclines".

Figures 3-5 and 3-6 show the relationship of birefringence and extinction angle χ to strain rate as obtained by Peebles, Prados and Honeycutt[17]. The data was obtained at 25.00°C, for different values of solution concentration.

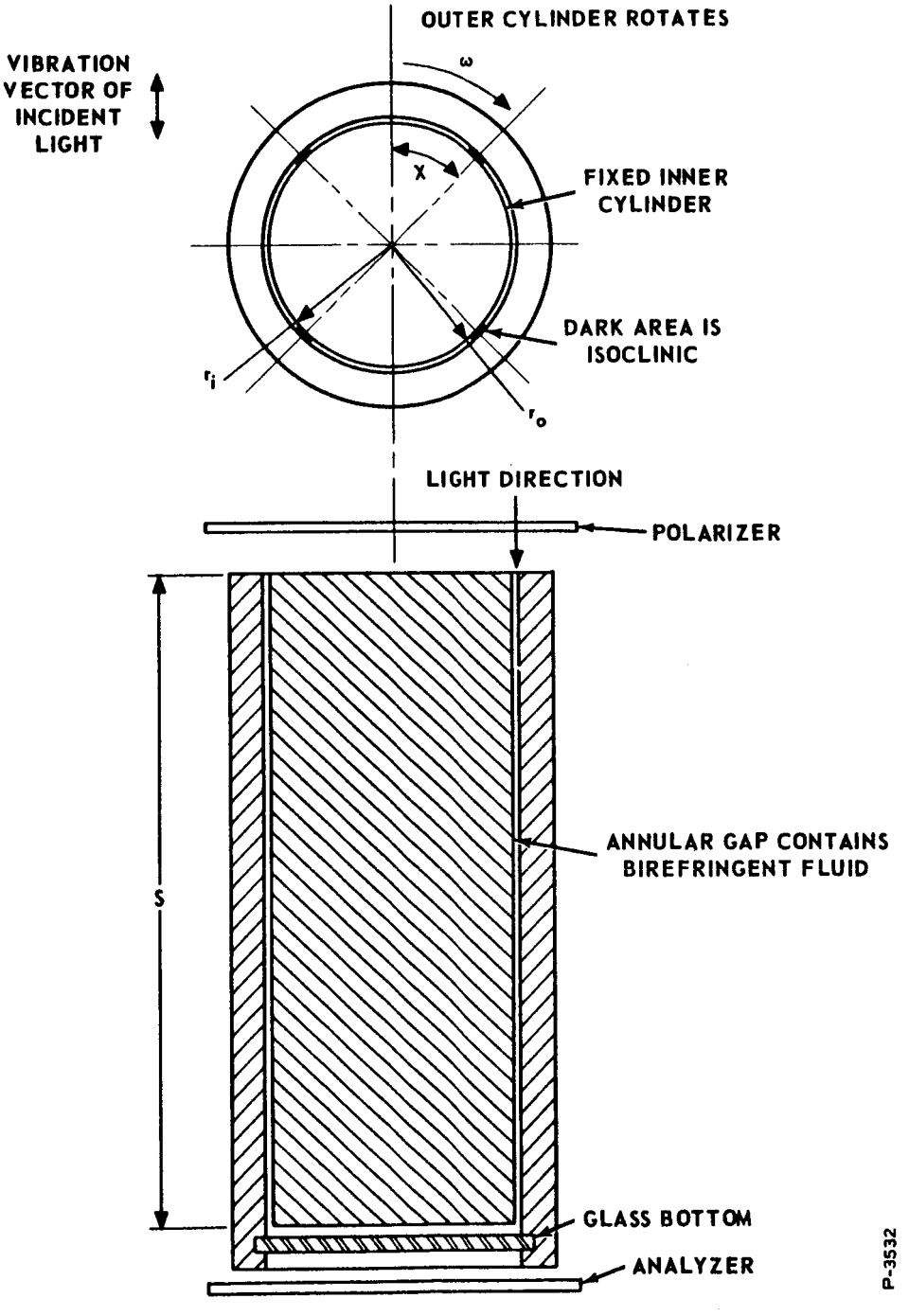

Figure 3-3 - Concentric Cylinder Polariscope

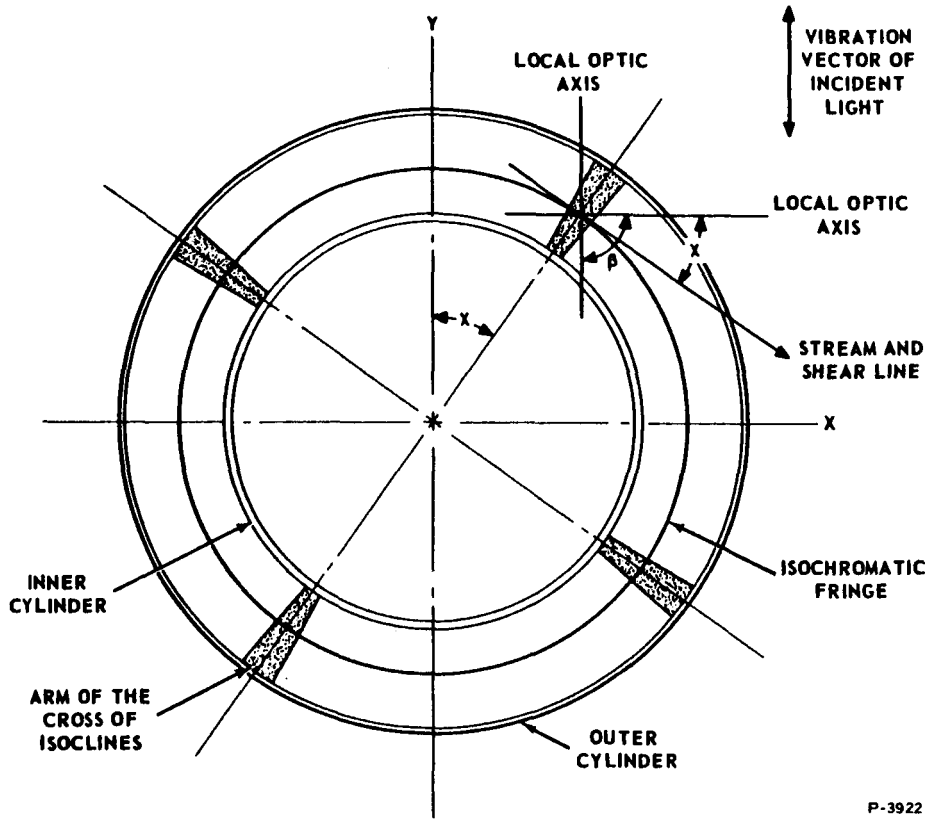

Figure 3-4 - Cross of Isoclines

It should be pointed out that the calibration curves of birefringence and extinction angle as a function of strain rate are not unique, but rather are dependent upon fluid temperature and condition of strain. The effect of temperature on the shear-optic relation was observed by Peebles, Prados, and Honeycutt[17]. Their observations were that a temperature increase caused a decrease in birefringence, while a temperature decrease caused an increase in birefringence, for the same value of shear rate. The sensitivity of the fluid properties to temperature change was noted for variations as small as 0.2 degree centigrade.

The strain condition effect was recently reported by Hirsch,[8] where he showed that the optic response of the fluid will be different, depending on whether the fluid is subjected to pure gliding strain (as in flow between parallel straight walls), or dilation strain (strain produced by convergence or divergence of the flow). Hirsch showed that the calibration curves of the fluid for the two different types of strain rate will coincide only up to a certain value of strain rate (as low as 10 sec^{-1}). Then the calibration curve will branch off into two distinct curves. The value of the strain rate at which this branching occurs has been identified

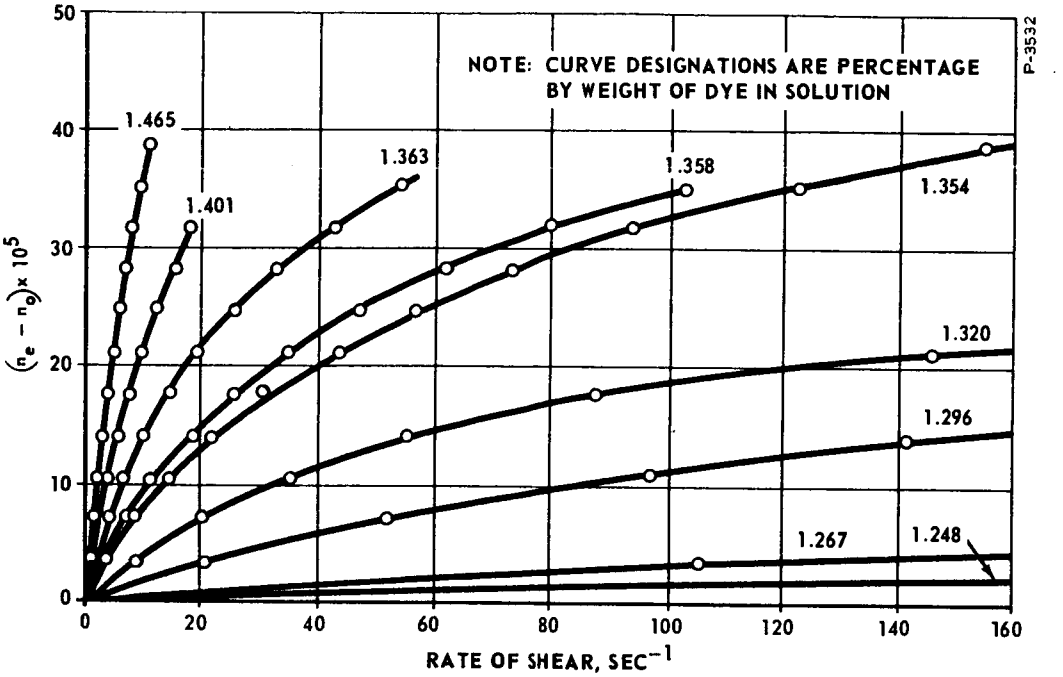

Figure 3-5 - Birefringence as a Function of Rate of Shear for Liquids Tested (From Reference 17)

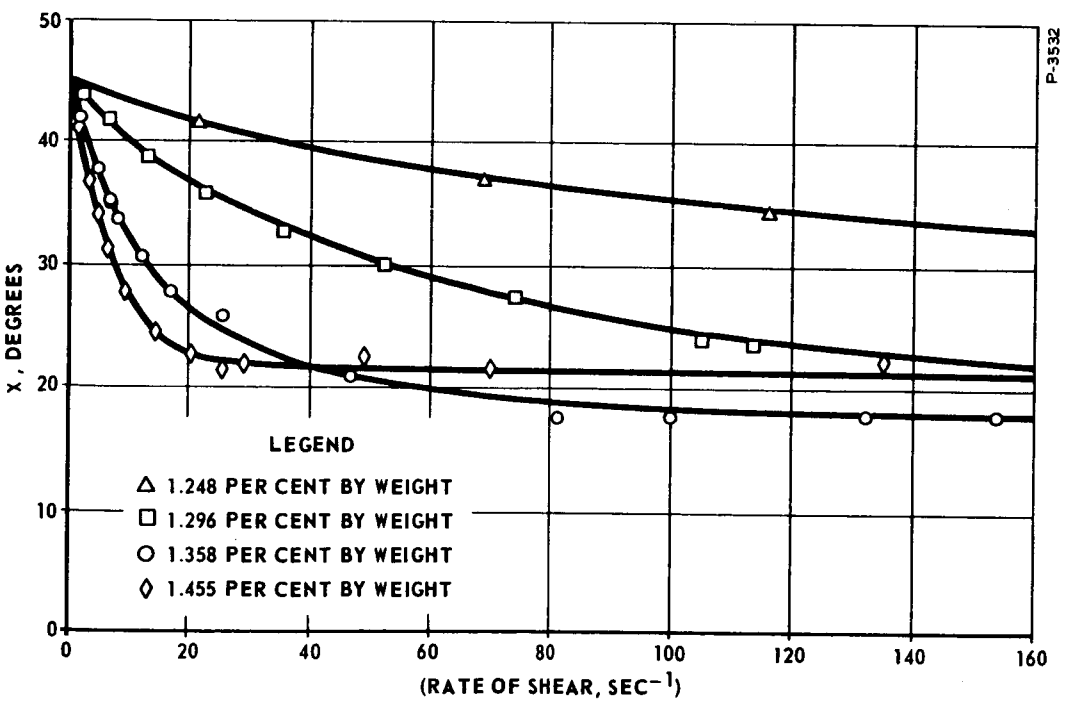

Figure 3-6 - Extinction Angle as a Function of Shear for Four Representative Solutions in a Moderate Shear Range (From Reference 17)

as the point where the fluid begins to exhibit a non-Newtonian behavior. It has been shown, however, that this "secondary" effect of the optic response of the fluid has negligible effect in determining the velocity profiles in the flow, but does affect the accuracy of the technique in obtaining the stress distribution in the flow field.

3.4 FLUID MECHANICS CONSIDERATIONS

It has been stated previously that the relationship between birefringence and strain rate in a doubly-refracting liquid can be expressed as

$$|n_e - n_o| = \lambda \mu M E_{max} \tag{3.14}$$

It is assumed that the deformation rates are low enough that the "branching" effect on the optical response, referred to above, is not encountered. It is expedient at this time to determine the relation between E_{max}, the maximum rate of deformation, and the velocity gradients that exist in the flow field.

A small element of fluid is shown in Figure 3-7, subjected to a generalized system of stresses. The shear stress acting on a plane of unit length inclined at an angle ξ to the horizontal may be obtained by a force balance on the element shown in Figure 3-8. Summing the forces in the direction of shear stress, we obtain

$$\tau_\xi A + \sigma_x A \sin\xi \cos\xi - \sigma_y A \cos\xi \sin\xi + \tau_{yx} A \sin\xi \cos\xi - \tau_{xy} A \cos\xi \sin\xi = 0 \tag{3.17}$$

P-3922

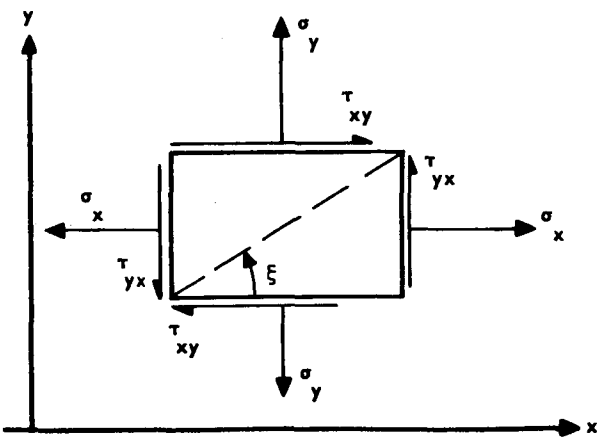

Figure 3-7 - Fluid Element Subjected to a Generalized Two-Dimensional Stress System

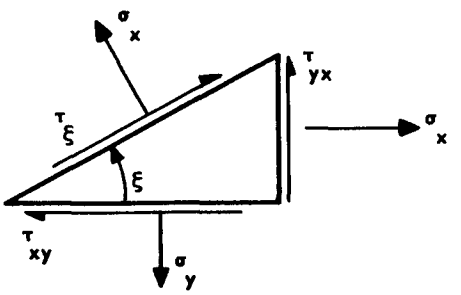

Figure 3-8 - Resolution of Combined Stresses

Collecting like terms and utilizing some trigonometric identities, we obtain

$$\tau_{\xi} = \frac{(\sigma_y - \sigma_x)}{2} \sin 2\xi + \tau_{xy} \cos 2\xi \qquad (3.18)$$

since

$$\tau_{xy} = \tau_{yx}$$

From the Navier-Stokes development of shear and normal stress in terms of velocity derivatives, we obtain

$$\sigma_x = -p + 2\mu \frac{\partial u}{\partial x} \qquad (3.19a)$$

$$\sigma_y = -p + 2\mu \frac{\partial v}{\partial y} \qquad (3.19b)$$

$$\tau_{xy} = \mu \left(\frac{\partial u}{\partial y} + \frac{\partial v}{\partial x} \right) \qquad (3.19c)$$

where u and v are the velocity components in the x and y directions respectively, p is the hydrostatic pressure, and μ is the fluid viscosity. Substituting these relations into equation (3.18), we have

$$\tau_{\xi} = \mu \left(\frac{\partial v}{\partial y} - \frac{\partial u}{\partial x} \right) \sin 2\xi + \mu \left(\frac{\partial v}{\partial x} + \frac{\partial u}{\partial y} \right) \cos 2\xi. \qquad (3.20)$$

Equation (3.20) becomes more flexible if the coordinate system is transformed from the cartesian system to a stream coordinate system. The relationships between the two coordinate systems can be obtained from Figures 3-9(a) and 3-9(b).

$$s = x \cos \phi + y \sin \phi \qquad (3.21a)$$

$$n = -x \sin \phi + y \cos \phi \qquad (3.21b)$$

$$u = V \cos \phi \qquad (3.21c)$$

$$v = V \sin \phi \qquad (3.21d)$$

where

ϕ = angle between streamline and x-axis

s = distance along streamline

n = distance along normal to streamline

V = velocity along streamline

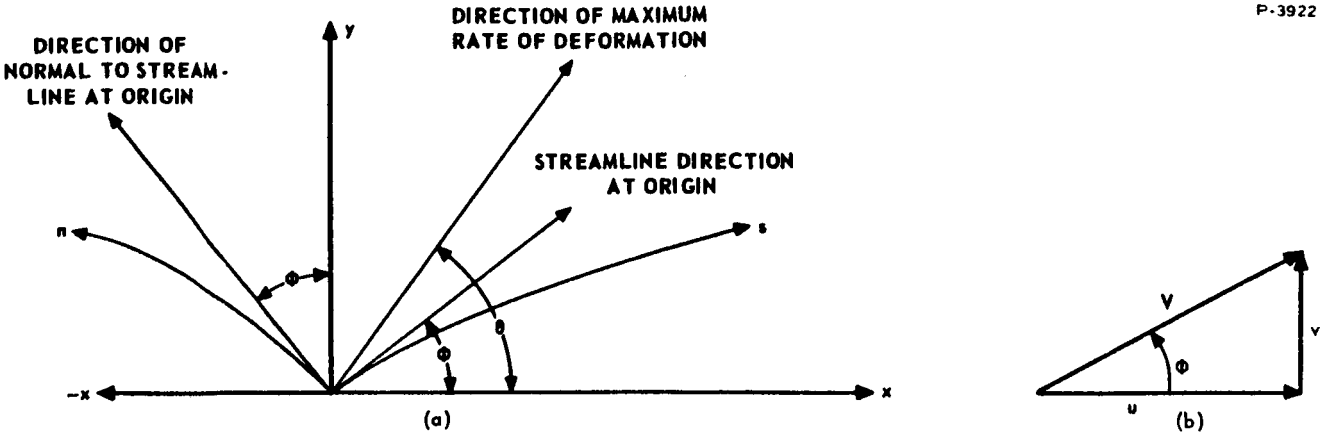

Figure 3-9 - Directional Relationships in Two-Dimensional Flow Field

If we have some variable f which is a function of s and n, which in turn are functions of x and y, one can write that since

$$d f = \frac{\partial f}{\partial s} d s + \frac{\partial f}{\partial n} d n \qquad (3.22a)$$

then

$$\frac{\partial f}{\partial x} = \frac{\partial f}{\partial s}\frac{\partial s}{\partial x} + \frac{\partial f}{\partial n}\frac{\partial n}{\partial x} \qquad (3.22b)$$

$$\frac{\partial f}{\partial y} = \frac{\partial f}{\partial s}\frac{\partial s}{\partial y} + \frac{\partial f}{\partial n}\frac{\partial n}{\partial y} \qquad (3.22c)$$

Substituting values for the partial derivatives of the stream coordinates with respect to the cartesian coordinates, equations (3.22b) and (3.22c) become

$$\frac{\partial f}{\partial x} = \cos\phi \frac{\partial f}{\partial s} - \sin\phi \frac{\partial f}{\partial n} \qquad (3.23a)$$

$$\frac{\partial f}{\partial y} = \sin\phi \frac{\partial f}{\partial s} + \cos\phi \frac{\partial f}{\partial n} \qquad (3.23b)$$

We can write that

$$\frac{\partial v}{\partial y} - \frac{\partial u}{\partial x} = \frac{\partial(V \sin\phi)}{\partial y} - \frac{\partial(V \cos\phi)}{\partial x}$$

$$= V \cos\phi \frac{\partial \phi}{\partial y} + \sin\phi \frac{\partial V}{\partial y} + V \sin\phi \frac{\partial \phi}{\partial x} - \cos\phi \frac{\partial V}{\partial x} \qquad (3.24)$$

since both ϕ and V are functions of x and y. Applying equations (3.23a) and (3.23b) to equation (3.24), we obtain

$$\frac{\partial v}{\partial y} - \frac{\partial u}{\partial x} = V \cos \phi \left[\sin \phi \frac{\partial \phi}{\partial s} + \cos \phi \frac{\partial \phi}{\partial n}\right] + \sin \phi \left[\sin \phi \frac{\partial V}{\partial s} + \cos \phi \frac{\partial V}{\partial n}\right]$$
$$+ V \sin \phi \left[\cos \phi \frac{\partial \phi}{\partial s} - \sin \phi \frac{\partial \phi}{\partial n}\right] - \cos \phi \left[\cos \phi \frac{\partial V}{\partial s} - \sin \phi \frac{\partial V}{\partial n}\right] \tag{3.25}$$

Combining like terms and applying trigonometric identities, we obtain equation (3.25) as

$$\frac{\partial v}{\partial y} - \frac{\partial u}{\partial x} = \left[\frac{\partial V}{\partial n} + \frac{V \partial \phi}{\partial s}\right] \sin 2\phi - \left[\frac{\partial V}{\partial s} - \frac{V \partial \phi}{\partial n}\right] \cos 2\phi \tag{3.26}$$

In a similar manner, we obtain

$$\frac{\partial u}{\partial y} + \frac{\partial v}{\partial x} = \left[\frac{\partial V}{\partial n} + \frac{V \partial \phi}{\partial s}\right] \cos 2\phi + \left[\frac{\partial V}{\partial s} - \frac{V \partial \phi}{\partial n}\right] \sin 2\phi \tag{3.27}$$

Substituting equations (3.26) and (3.27) into equation (3.20) gives

$$\tau_\xi = \mu \left\{\left[\frac{\partial V}{\partial n} + \frac{V \partial \phi}{\partial s}\right] \sin 2\phi - \left[\frac{\partial V}{\partial s} - \frac{V \partial \phi}{\partial n}\right] \cos 2\phi \right\} \sin 2\xi$$
$$+ \mu \left\{\left[\frac{\partial V}{\partial n} + \frac{V \partial \phi}{\partial s}\right] \cos 2\phi + \left[\frac{\partial V}{\partial s} - \frac{V \partial \phi}{\partial n}\right] \sin 2\phi \right\} \cos 2\xi \tag{3.28}$$

From the general definition of viscosity in two-dimensional flow, we have

$$E_\xi = \frac{\tau_\xi}{\mu} \tag{3.29}$$

Using equation (3.29) and combining like terms and simplifying in equation (3.28) gives

$$E_\xi = \left[\frac{\partial V}{\partial n} + \frac{V \partial \phi}{\partial s}\right] \cos (2\phi - 2\xi) + \left[\frac{\partial V}{\partial s} - \frac{V \partial \phi}{\partial n}\right] \sin (2\phi - 2\xi) \tag{3.30}$$

From Figure 3-9(a), we note that

$$\frac{\partial \phi}{\partial s} = -\frac{1}{r} \tag{3.31a}$$

$$\frac{\partial \phi}{\partial n} = \frac{1}{r'} \tag{3.31b}$$

where r and r' are the radii of curvature of the streamline and the normal to the streamline, respectively. This substitution into equation (3.30) yields

$$E_{\xi} = \left(\frac{\partial V}{\partial n} - \frac{\partial V}{\partial r}\right) \cos (2\phi - 2\xi) + \left(\frac{\partial V}{\partial s} - \frac{V}{r'}\right) \sin (2\phi - 2\xi) \tag{3.32}$$

In cartesian coordinates, the continuity equation for steady incompressible, two-dimensional flow is

$$\frac{\partial u}{\partial x} + \frac{\partial v}{\partial y} = 0 \tag{3.33}$$

In terms of stream coordinates, we obtain

$$\frac{\partial V}{\partial s} + \frac{V}{r'} = 0 \tag{3.34}$$

where equations (3.21) through (3.23) have been utilized to obtain the transformation.

Solving equation (3.34) for $\frac{\partial V}{\partial s}$ and substituting into equation (3.32), we obtain

$$E_{\xi} = \left(\frac{\partial V}{\partial n} - \frac{V}{r}\right) \cos (2\phi - 2\xi) - \frac{2V}{r'} \sin (2\phi - 2\xi) \tag{3.35}$$

If we differentiate equation (3.35) with respect to ξ and set the resultant to zero, we can find the orientation of the maximum shear stress. Performing this differentiation, we obtain

$$\frac{d E_{\xi}}{d \xi} = 0 = 2 \left(\frac{\partial V}{\partial n} - \frac{V}{r}\right) \sin (2\phi - 2\xi) + \frac{4V}{r'} \cos (2\phi - 2\xi) \tag{3.36}$$

By noting that $\xi = \theta$ from Figure 3-9a, we can solve equation (3.36) which gives

$$\tan (2\phi - 2\theta) = \frac{\frac{-2V}{r'}}{\frac{\partial V}{\partial n} - \frac{V}{r}} \tag{3.37}$$

Substituting this result into equation (3.35), we obtain after simplification that

$$E_{max} = \sqrt{\left(\frac{\partial V}{\partial n} - \frac{V}{r}\right)^2 + \left(\frac{2V}{r'}\right)^2} \qquad (3.38)$$

Equation (3.38) provides the desired relationship between the maximum rate of deformation and the velocity gradient normal to the streamline. The equation can be rearranged to solve for the gradient in terms of the maximum strain rate, since this is the quantity obtained from the isochromatics in birefringent measurements. Solving, we obtain

$$\frac{\partial V}{\partial n} = \frac{V}{r} \pm \sqrt{E_{max}^2 - \frac{4V^2}{r'^2}} \qquad (3.39)$$

Equation (3.39) is of limited value in solving for velocity profiles, since it requires prior knowledge of the radii of curvature of the stream and normal curves. That is, the stream pattern must be known throughout the field before equation (3.39) can be used to solve for the velocity profiles. In a general flow field, this information is not known ahead of time.

The application of equation (3.39) to two special flow cases will be demonstrated here. In Figure 3-10(a), the flow is straight and parallel, corresponding to a condition of pure gliding strain, while in Figure 3-10(b), the flow is diverging. A condition of pure dilation strain is obtained at the centerline of the channel.

In Figure 3-10(a), the streamlines and the normals are all straight lines, having infinite radii of curvature r and r'. If we substitute these numerical values into equation (3.39), we obtain

$$\frac{\partial V}{\partial n} = \pm E_{max}.$$

In Figure 3-10(b), the streamlines are straight, indicating that the corresponding radii of curvature are infinite. The normal lines, however, have radii of curvature r' equal to the radius to the normal line in question from the geometric point of divergence. In addition, we have that the $\frac{\partial V}{\partial n}$ at the channel centerline is zero. If we substitute these values into equation (3.39), we get

$$\frac{V}{r'} = \pm E_{max}$$

corresponding to a condition of pure dilation strain on the centerline.

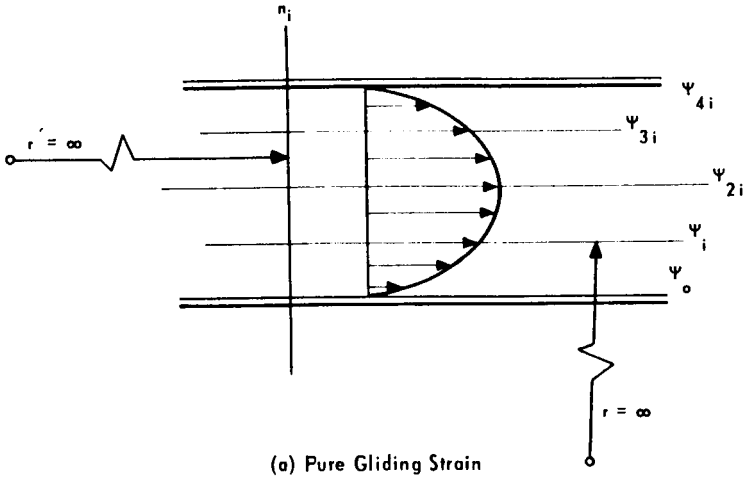

(a) Pure Gliding Strain

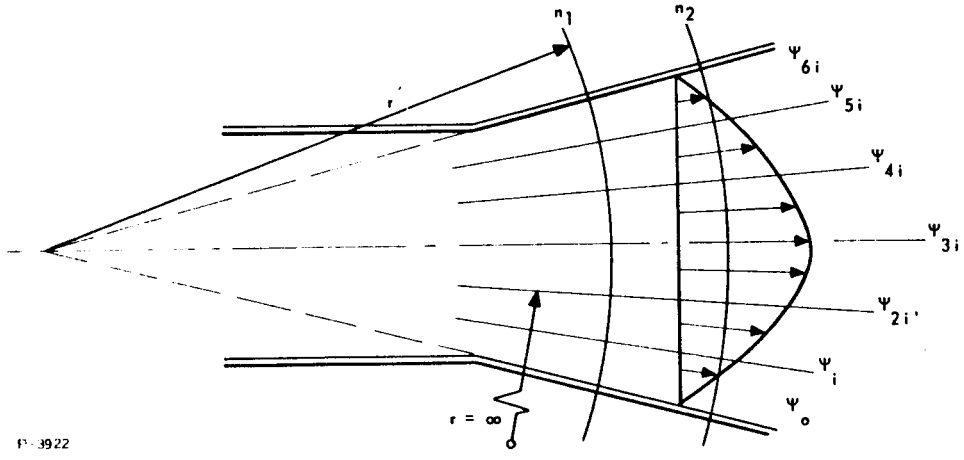

(b) Pure Dilation Strain At Channel Centerline

Figure 3-10 - Two Basic Types of Shear Strain

If we rewrite equation (3.37) by taking the inverse tangent of both sides, we obtain the relation between the direction of the maximum deformation and the streamline.

$$2\phi - 2\theta = \tan^{-1}\left[\frac{\frac{-2V}{r'}}{\frac{\partial V}{\partial n} - \frac{V}{r}}\right] \qquad (3.40)$$

This equation shows that the streamline coincides with the direction of maximum shear only for the case where the normal curves to the streamlines are straight lines, which means that no divergence or convergence

of the flow field is occurring. Additionally, it indicates that the maximum angle that can occur between the streamline and maximum shear directions is 45 degrees. This condition would occur along the centerline of a converging or diverging channel. Since the isoclinic fringe directions are determined by the direction of the maximum rate of deformation E, the isoclinics are of little use in determining the streamline patterns where convergence or divergence of the flow occurs. Hence, equations (3.39) and (3.40) are only of use when:

(1) the streamline pattern is known from the channel configuration

(2) it is known that no convergence or divergence of the flow occurs, or when

(3) the streamline patterns can be obtained by some other method, such as dye injection.

In any one of the three cases indicated above, the velocity profile can be obtained by graphical integration of equation (3.39), and utilizing the boundary condition that V = 0 on the channel walls.

A method for analyzing a general two-dimensional flow case where the streamlines are unknown and are neither straight nor parallel, has been suggested by Rosenberg[20]. It has been recently refined by Peebles and Liu[16] to a degree where the isoclinics are no longer needed, and the streamlines can be determined entirely from the isochromatic locations.

The analysis requires the introduction of the Stokes stream function ψ defined as

$$u = \frac{-\partial \psi}{\partial y} \tag{3.41a}$$

$$v = \frac{\partial \psi}{\partial x} \tag{3.41b}$$

We have shown previously that the shear stress on any plane inclined at an angle ξ with respect to the x-axis is given by

$$\tau_{\xi} = \mu \left(\frac{\sigma_y - \sigma_x}{2} \right) \sin 2\xi + \tau_{xy} \cos 2\xi \, . \tag{3.18}$$

If we differentiate this expression with respect to ξ and set the derivative equal to zero, we obtain

$$\tan (2\,\xi)_{max} = \frac{\sigma_y - \sigma_x}{2\,\tau_{xy}} \tag{3.42a}$$

From trigonometric identities, we further obtain

$$\sin (2\,\xi)_{max} = \frac{\sigma_y - \sigma_x}{\sqrt{\left(\sigma_y - \sigma_x\right)^2 + \left(2\,\tau_{xy}\right)^2}} \tag{3.42b}$$

$$\cos (2\,\xi)_{max} = \frac{2\,\tau_{xy}}{\sqrt{\left(\sigma_y - \sigma_x\right)^2 + \left(2\,\tau_{xy}\right)^2}} \tag{3.42c}$$

where ξ_{max} is the direction of maximum shear stress with respect to the positive x-axis.

Substituting equations (3.42a, b and c) into equation (3.18) gives

$$\tau_{max} = \sqrt{\frac{\left(\sigma_y - \sigma_x\right)^2}{2} + \left(\tau_{xy}\right)^2} \tag{3.43}$$

which becomes

$$\tau_{max} = \mu \sqrt{\left(\frac{\partial v}{\partial y} - \frac{\partial u}{\partial x}\right)^2 + \left(\frac{\partial u}{\partial y} + \frac{\partial v}{\partial x}\right)^2} \tag{3.44}$$

upon substitution of equations (3.19a, b and c). The right hand side of equation (3.44) is identically equal to the product of the viscosity and the maximum rate of deformation, $\mu\, E_{max}$. From equation (3.33), we can write

$$\frac{\partial v}{\partial y} = -\frac{\partial u}{\partial x} \,. \tag{3.45}$$

Therefore, we can express E_{max} by

$$E_{max} = \sqrt{4\left(\frac{-\partial u}{\partial x}\right)^2 + \left(\frac{\partial u}{\partial y} + \frac{\partial v}{\partial x}\right)^2} \tag{3.46}$$

Substituting from equations (3.41a and b), equation (3.46) becomes

$$E_{max} = \sqrt{\left(\frac{-2\partial^2 \psi}{\partial x\, \partial y}\right)^2 + \left(\frac{\partial^2 \psi}{\partial y^2} - \frac{\partial^2 \psi}{\partial x^2}\right)^2} \qquad (3.47)$$

The measured values of E_{max} are obtained directly from the observed isochromatic patterns formed over the flow field. The calculations for the values of the stream function throughout the flow field can be carried out conveniently by writing equation (3.47) in finite difference form and solving by numerical iteration. Boundary conditions can be obtained from known values of the stream function along solid boundaries.

It has been shown previously that the velocity gradient in terms of stream coordinates is related to the maximum rate of deformation in the fluid by

$$\frac{\partial V}{\partial n} = \frac{V}{r} \pm \sqrt{E_{max}^2 + \frac{4\, V^2}{r'^2}} \qquad (3.39)$$

where r and r' are the radii of curvature of the streamline and normal to the streamlines, respectively. If we consider the case of laminar flow between straight parallel walls, r and r' become infinite, and equation (3.39) simplifies to

$$\frac{\partial V}{\partial n} = \pm E_{max} \qquad (3.48)$$

For this particular flow case, equation (3.40) becomes

$$2\phi - 2\theta = 0 \qquad (3.49)$$

which indicates that the streamlines are coincident with the direction of the maximum rate of deformation.

This type of flow is most simply obtained in a rectangular channel of high aspect ratio, where the aspect ratio is defined as channel depth-to-height. For the high aspect ratio channel flow, the velocity profile is essentially one-dimensional and, for a constant viscosity, can be expressed as

$$u = U_o \left(1 - \frac{y^2}{h^2}\right) \qquad (3.50)$$

where

U_o = velocity along the channel centerline

h = the half-height of the channel

y = vertical distance measured from the centerline of the channel as shown in Figure 3-11

From a consideration of equations (3.19a, b and c), we find that the stress existing in the fluid is

$$\tau_{xy} = \mu \left(\frac{\partial u}{\partial y}\right) = -2 \mu U_o \frac{y}{h^2} \tag{3.51}$$

since $v = 0$. If we divide both sides by μ, we get

$$\frac{\partial u}{\partial y} = -2 U_o \frac{y}{h^2} \cdot \tag{3.52}$$

Since $\frac{\partial u}{\partial y} \equiv \frac{\partial V}{\partial n}$, we can equate the magnitude of the maximum rate of deformation to the flow in the channel. If we do this, we obtain

$$E_{max} = \pm 2 U_o \frac{y}{h^2} \cdot \tag{3.53}$$

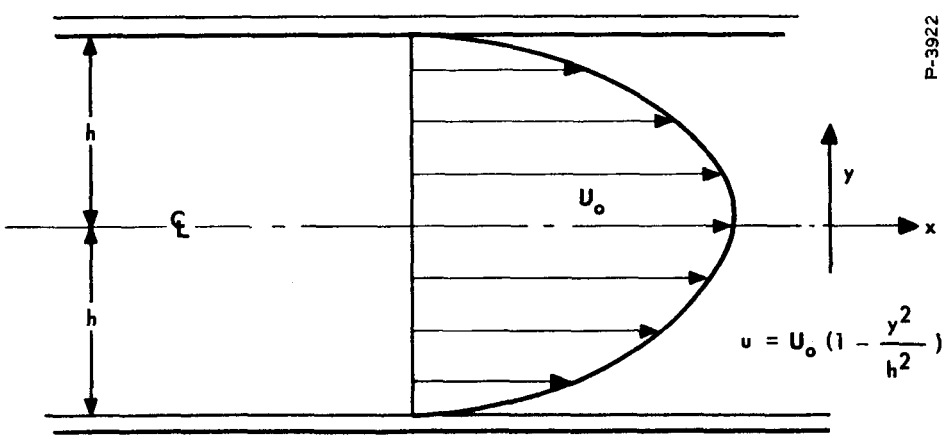

Figure 3-11 - Fully-Developed Laminar Flow in a Rectangular Channel

One further simplification of the above equation can be made by noting that for a rectangular channel,

$$U_o = \frac{3}{2} \frac{Q}{A} \tag{3.54}$$

where Q is the volume flow rate, and A is the cross-sectional area of the channel (L x 2h). Equation (3.54) can be obtained from

$$Q = \int_A u \, d A = 2 U_o \int_o^h \left(1 - \frac{y^2}{h^2}\right) L \, d y. \tag{3.55}$$

Substituting equation (3.54) into (3.53) gives

$$E_{max} = \pm 3 \left(\frac{Q}{A}\right) \frac{y}{h^2} \cdot \tag{3.56}$$

The convenience of equation (3.56) can be realized when it is considered that the locations of the fringes in the rectangular channel can be obtained in permanent form by taking a photograph of the channel. By recording the volume flow rate corresponding to the particular photograph, the magnitude of the maximum deformation rate can be calculated from equation (3.56) corresponding to the location of each fringe. In this manner, one can obtain a plot of fringe order N versus E_{max}. By utilizing equation (3.16), one can then obtain the fluid calibration of birefringence $(n_e - n_o)$ versus maximum rate of deformation E.

From a system standpoint, the use of a rectangular channel to obtain the optical response of a fluid rather than a concentric cylinder polariscope provides a great deal of convenience. One very attractive feature is that the channel can be plumbed into the system in either series or parallel with the test model, allowing a calibration fluid curve to be obtained at any time without breaking any hydraulic connections. Secondly, the problem of reproducing temperature conditions is much less severe than that encountered with the polariscope. The temperature regulator of the main system will provide a constant temperature flow through the calibration channel for an indefinite length of time. Thirdly, there is no necessity to procure optical equipment in addition to the photoviscous test stand proper, and the cost of the calibration channel is far less than the cost of the rotating concentric cylinders alone.

It is necessary to point out here that the use of the rectangular channel for obtaining the shear optic relation for a fluid requires fully developed parabolic flow in the channel. An important consideration for flow in a rectangular channel is the length from the entrance required to establish the parabolic velocity distribution described by equation (3.50). From Reference (19),

$$\frac{\nu\, x_d}{\bar{u}\, h^2} = 0.08 \tag{3.57}$$

where

x_d = length for development of velocity distribution, in

ν = kinematic viscosity, in^2/sec

$\bar{u}$ = average velocity, in/sec

h = channel half-height, in

Using the relationship

$$\bar{u} = \frac{Q}{2\, h\, L}$$

where

L = channel depth, measured along light path, in

Q = flow rate, in^3/sec

we obtain

$$\frac{x_d}{h} = \frac{Q}{2\, \nu\, L} \tag{3.58}$$

This expression can be used to predict the length required for fully developed flow in a rectangular channel for a given set of experimental conditions.

If the fluid is in a non-Newtonian flow range, the velocity distribution will not have the parabolic form indicated by equation (3.50). (Appendix C is a treatment of non-Newtonian flow in a rectangular channel.) As a consequence of the modified velocity distribution, the deformation rate E will not vary linearly from the channel centerline to the wall as described by equation (3.53). Thus, in a non-Newtonian

case, we would expect the isochromatic fringes to be unequally spaced across the channel. The uniformity of fringe spacing then could serve as a check on whether the flow in the channel is or is not Newtonian. However, uniformity of fringe spacing would not be a satisfactory criterion if a non-linearity in the $(n_e - n_o)$ versus E relationship happened to compensate the effect of the variation of μ with E.

A better method of checking if the flow is Newtonian is by rheological data. This could be obtained by measuring the pressure drop versus flow rate relationship over a length of the channel, or across a constant-area capillary passage, with the flow non-turbulent. If the pressure drop versus flow rate relationship is linear, the flow is Newtonian in the range examined. Figure 3-12 shows typical rheological curves obtained for various concentrations of Milling Yellow dye (from Reference 17).

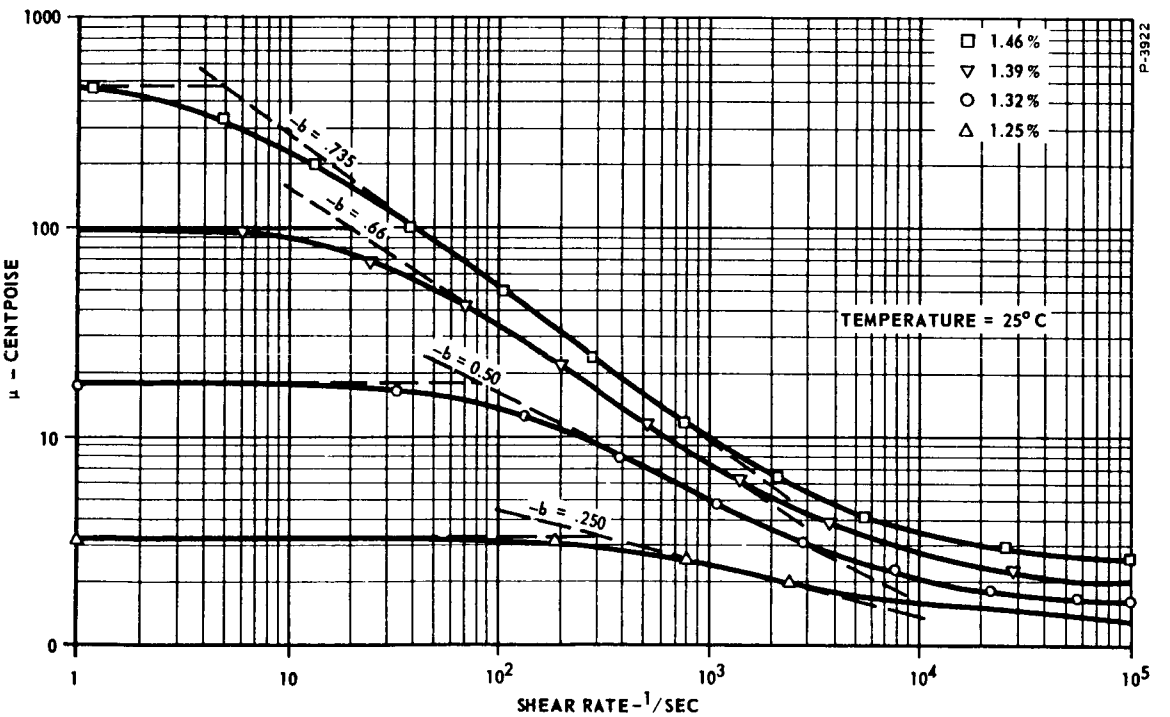

Figure 3-12 - Variation of Viscosity with Shear Rate for Various Concentrations of Milling Yellow Dye (From Reference 17)

SECTION 4

EXPERIMENTAL PROGRAM

4.1 PHOTOVISCOUS TEST EQUIPMENT

The equipment required to produce visible fringe patterns in a photoviscous fluid is really very basic and very inexpensive. The phenomenon can be observed by simply shaking a sample of the fluid in a glass bottle placed between crossed polarized sheets and illuminated by an ordinary light bulb. However, if the technique is intended for detail examination of flow patterns in specific two-dimensional flow fields, the hardware requirements become more sophisticated.

The equipment required for obtaining quantitative data by the photoviscous technique can be thought of as two separate systems. One system is comprised of the optical components, while the other consists of all of the equipment needed for the fluid circulation system. Both will be discussed in the order indicated.

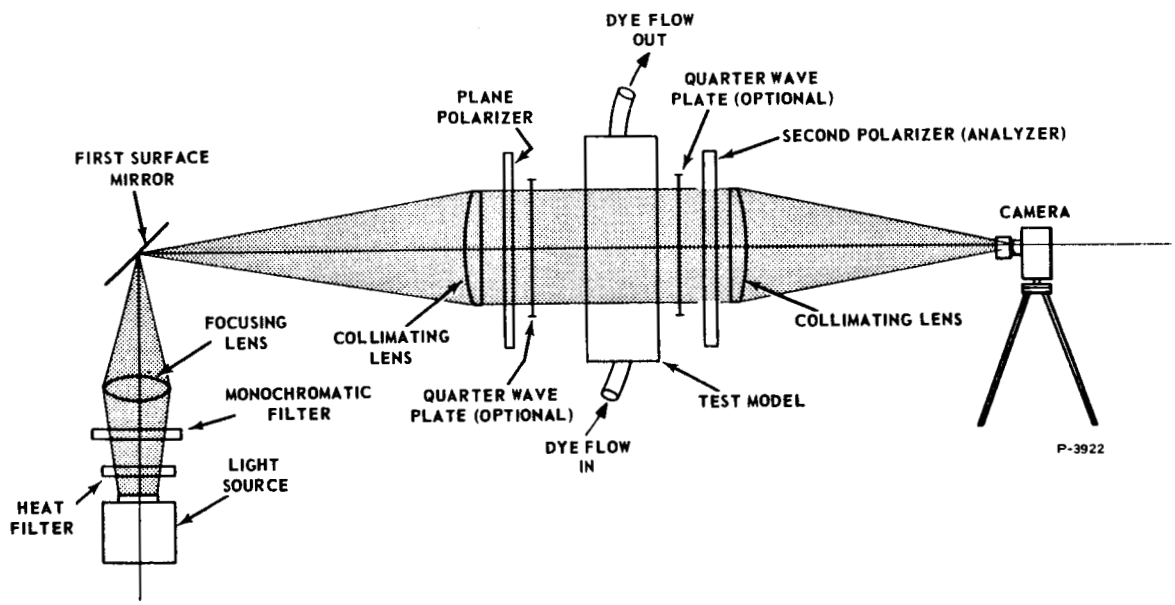

Figure 4-1 - Schematic of Optical System

The basic function of the optical system is to produce polarized light at an intensity such that the fringe patterns in the flow model can be easily visualized and easily photographed. The optical components involved in this function are shown schematically in Figure 4-1. The actual apparatus arrangement is shown in Figures 4-2 and 4-3. The light source and the heat filter are combined in one unit. The lamp produces white light and is rated at 150 watts. A fan is also enclosed in the unit to provide circulation of air around the bulb. The heat filter removes that part of the spectrum in the infra-red region, and is used to protect the monochromatic filter.

The focus lens and the monochromatic filter are also in one unit. The monochromatic filter passes only the green wavelength, and can be easily removed from the optical path to obtain white light. The focus lens assembly is used to provide an intense beam of light at the first surface mirror. The focus lens and the monochromatic filter are mounted in a sliding track so that the lens can be positioned to provide a minimum amount of dispersion at the mirror.

The collimating lenses produce a collimated bundle of light rays; that is, there is no convergence or divergence of the light beam. One lens is located at its focal distance from the mirror, and the other lens is used to provide a point image at the camera lens.

The polarizing sheets are purchased items from the Polaroid Corporation, and are actually a combination of a polarizer and a quarter wave plate. When light passes through in one direction, a sheet acts as a plane polarizer. When the sheet is reversed with respect to the light direction, circularly polarized light is obtained. However, if the circularly polarized mode is used, the light beam must undergo a reflection after passing through the polarizer. This is required by the particular construction of the combination quarter wave and polarizing sheet material used for both the polarizer and analyzer in the equipment. The reflection reverses the sense of rotation of the light vibration vector in the circularly-polarized beam. The reversal is necessary for the circularly polarized light to be converted to plane polarized light of the proper orientation in the analyzer.

The camera used for all of the experimental work was a Honeywell Pentax 35 mm single lens reflex, equipped with a 55 mm focal length

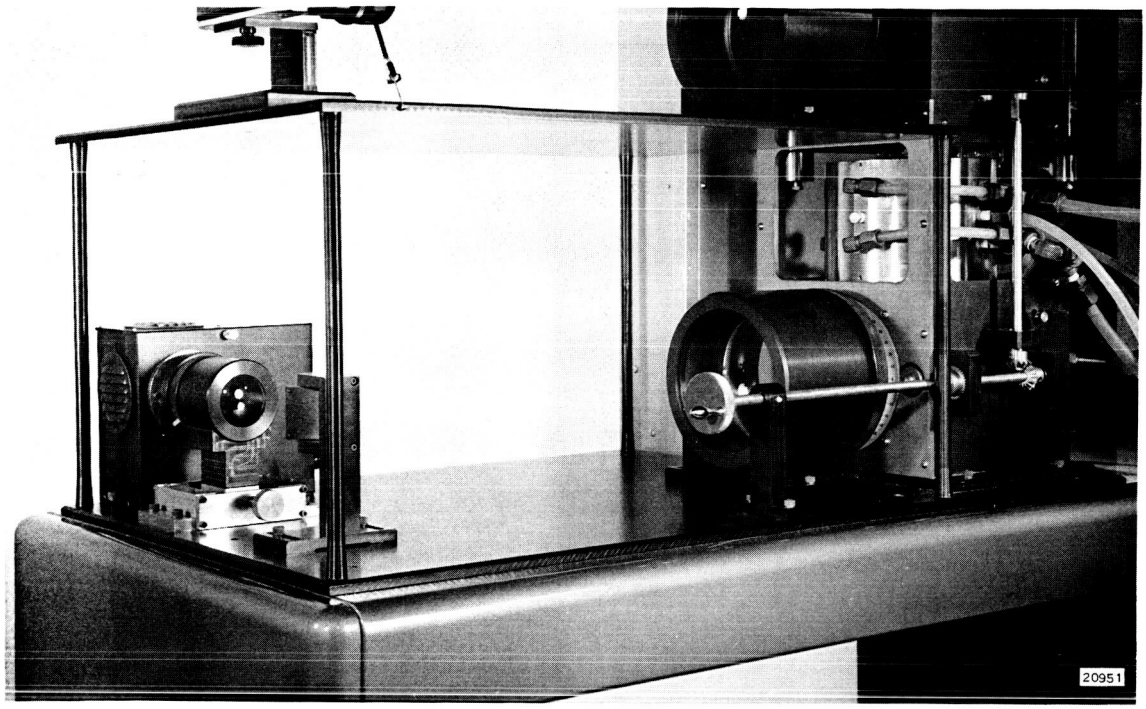

Figure 4-2 - Lower Optical Deck and Polaroid Fixture

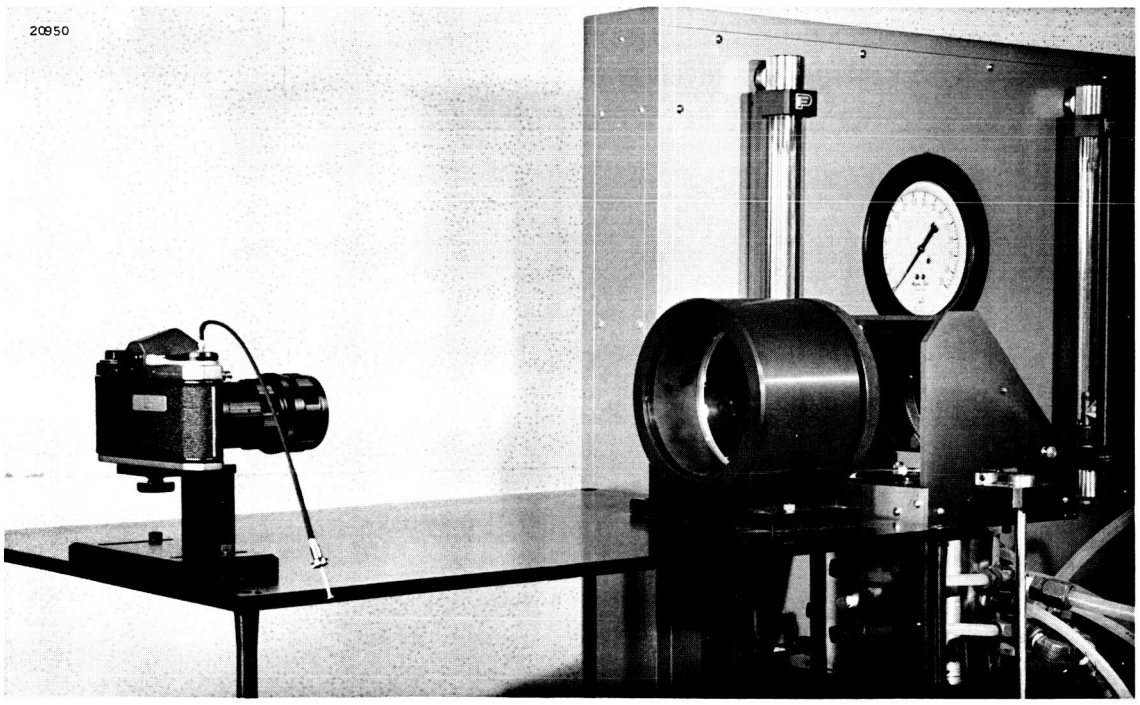

Figure 4-3 - Upper Optical Deck and Polaroid Fixture

f/2 Takumar lens in combination with a Spiratone 3x Telextender lens. Kodax Tri-X film ASA-400 was used for photographing the fringe patterns.

All of the optical equipment is mounted rigidly in fixtures which are bolted directly to aluminum base plates. The lower plate holds the light source, the lens assembly, the pivot mirror and the first collimator. The upper plate holds the second collimator and an adapter for the camera. The polarizer and analyzer and two first surface mirrors are contained in a structure which also serves as a holder for the test models. This structure is equipped with a hand crank which allows rotation of the polarizer and analyzer together so that isoclinic photographs at different orientations can be taken.

The fluid circulation system is shown schematically in Figure 4-4. The source of power is a centrifugal pump and motor combination manufactured by Oberdorfer Company. The motor delivers 1/3 horsepower at 3450 rpm, and the pump supplies 17 gallons per minute at 10 psig discharge pressure. The impeller and the casing are bronze.

The settling chamber is a stainless steel cylinder with a 1.5 gallon capacity. The settling chamber is used to decrease the velocity of the fluid so that the temperature may be sensed as accurately as possible.

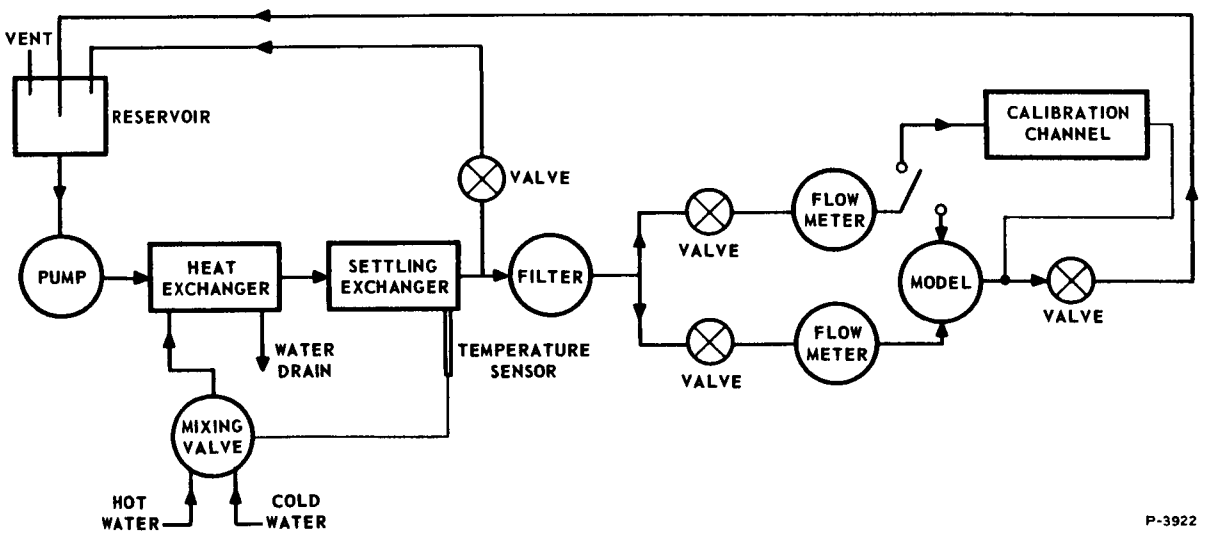

Figure 4-4 - Schematic of Flow Circulation System

The temperature of the Milling Yellow solution is regulated with a Jordan mixing valve and temperature sensor and a Vickers shell-and-tube heat exchanger. A schematic diagram of the mixing valve is shown in Figure 4-5.

The temperature regulation uses the feedback principle. From the Figure we see that the desired temperature setting is obtained by positioning a spring K_s which varies the load on diaphragm A_1. Assume the valve is at steady-state. Now, if a small decrease in the dye solution temperature T_f should occur, the pressure P_1 will decrease a corresponding amount. Alternatively, an increase in the valve setting T_{set} can be made manually. Either case violates the force balance between the pressure P_1 times the area A_1 of the diaphragm, and the spring load. Due to the resulting unbalance, the diaphragm will move up until a force equilibrium is achieved. The motion of the diaphragm is transmitted directly to the sliding valve, which, as shown in Figure 4-5, causes an increase in the valve area for the hot water flow and a decrease in the valve area for the cold water flow. Due to the net increase in enthalpy of the output flow to the heat exchanger, an increase in dye solution

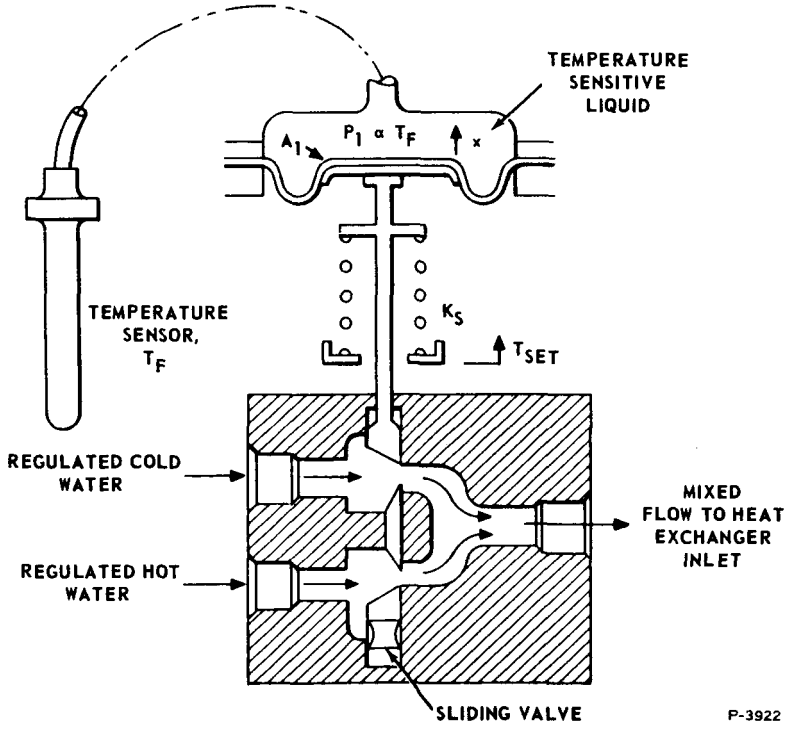

Figure 4-5 - Mixing Valve for Temperature Control

temperature is effected. The temperature of the solution continues to increase until the fluid in the sensor reaches a temperature level that produces a pressure force great enough to overcome substantially the initial force unbalance. The valve has now reached a new steady-state position with the error between commanded and actual fluid temperatures at a very small value.

The cold and hot water are supplied to the valve by Norgren pressure regulators, which tend to hold a constant differential pressure across the sliding valve. It can be seen that the feedback principle used in regulating the temperature will also minimize changes in dye solution temperature due to variations in water temperature.

Figure 4-6 represents the regulator system in block diagram form, where

$\frac{\partial F}{\partial T_{set}}$ = Change in spring load to change in desired fluid temperature

K_s = Spring rate of the bias spring

$\frac{\partial A_v}{\partial X}$ = Change in valve area with respect to travel

K_v = Turbulent flow coefficient of the sliding valve

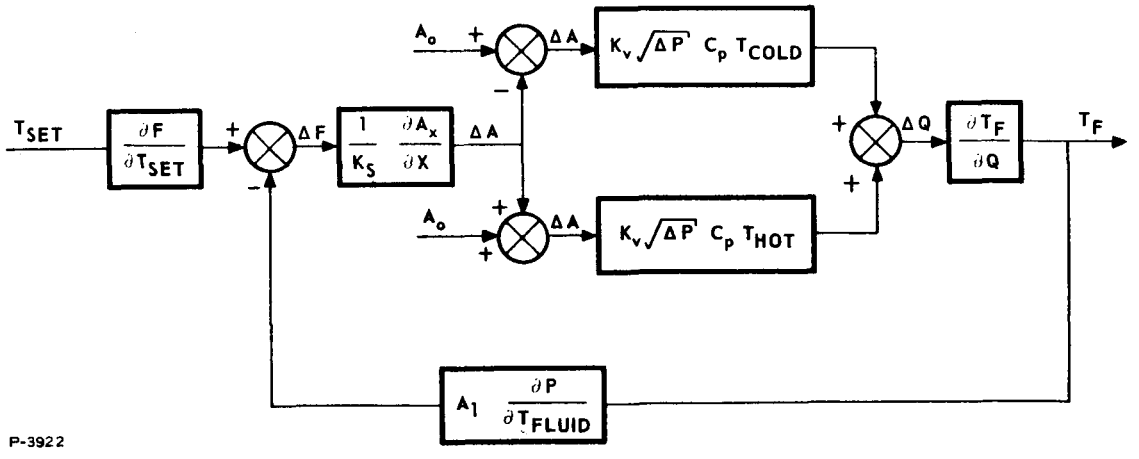

Figure 4-6 - Block Diagram of Temperature Regulating System

ΔP	=	Pressure drop across the valve
C_p	=	Specific heat at constant pressure
T_{cold}	=	Inlet temperature of the cold water
T_{hot}	=	Inlet temperature of the hot water
$\frac{\partial T_f}{\partial Q}$	=	Heat exchanger transfer function, change in output fluid temperature for a change in heat input
A_1	=	Area of diaphragm
$\frac{\partial P}{\partial T}_{fluid}$	=	Change in pressure of liquid in the sensor for a change in sensed fluid temperature.

The dye flowing from the heat exchanger can be split into two supply lines, each line having its own flowmeter. The flowmeters are manufactured by Fischer-Porter Co. and are calibrated in percent of volume flow. At 25°C, the 100 percent flow point corresponds to 5.85 in^3 per second of water. The tube assemblies are made of stainless steel and glass, and the floats are of stainless steel.

The supply tank is a purchased item from Tamco Products. The tank and spigot are made of polyeurethane, and the tank has a 5 gallon capacity. The return lines to the tank enter through drilled holes in the cap. The holes are slightly larger than the tube diameters so that the tank will essentially be vented to atmosphere while the amount of evaporation is minimized.

The lines and fittings connecting the hydraulic components are stainless steel and plastic. All of the dye flowing through the model is filtered down to 40 microinches by a Culligan filter located on the discharge side of the heat exchanger.

4.2 TEST MODELS

The bulk of the quantitative testing performed with the Milling Yellow dye was done on a rectangular channel of high aspect ratio and a model of a fluid state vortex valve. A description of both of these models will be given here.

The rectangular channel, which was used primarily for obtaining the optic response of the fluid, is shown in Figure 4-7. The channel was fabricated entirely of plexiglass. All of the side walls are 1/4 in. stock. The assembly was bonded together with clear cement, and machine screws were used to ensure sealing.

The model of the fluid state vortex valve is shown in Figure 4-8. This model also was fabricated entirely from plexiglass. The critical dimensions are indicated in the Figure. The height h of the mixing area in the vortex field is adjustable from 0.125 to 0.312 inch. The supply flow is introduced by four equally spaced fittings around the outside of the model. The control flow enters a plenum chamber supplying twelve equally spaced 0.030 tangential jet openings around the periphery of the vortex mixing chamber.

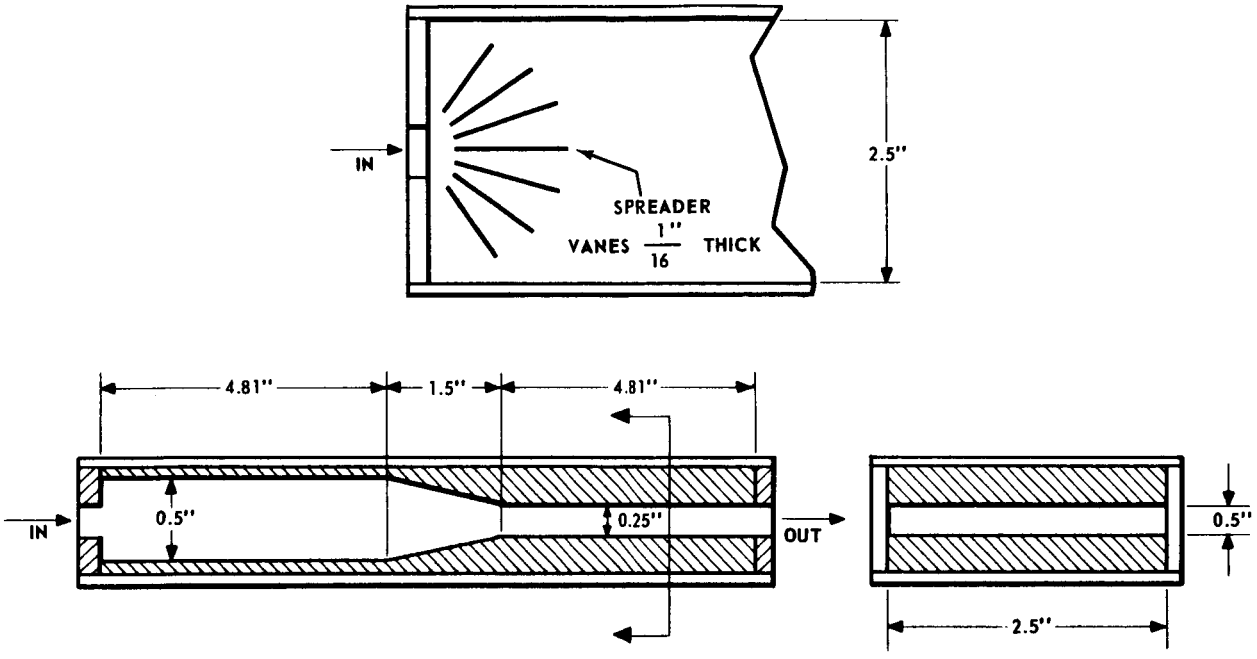

Figure 4-7 - Rectangular Channel Dimensions

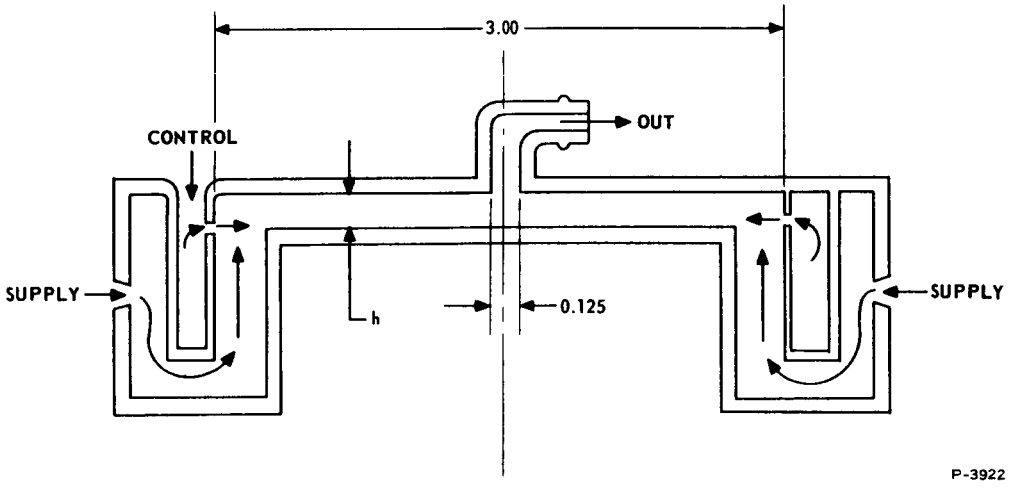

Figure 4-8 - Vortex Valve Dimensions

SECTION 5

EXPERIMENTAL PROGRAM

The scope of our experimental investigation was basically two-fold. The first objective was to show that the rectangular channel described previously could be used in lieu of a concentric cylinder polariscope to obtain the optic response of the doubly-refracting fluid. Our second objective was to determine the applicability of the photoviscous technique in obtaining velocity profiles in fluid state devices. This determination was to be based on a correlation between the velocity and shear distribution in a vortex valve with pure radial flow, obtained by the photoviscous technique, and that distribution predicted from analytical considerations. The technique followed in the investigation will be presented in the following discussion.

5.1 PREPARATION FOR TESTS

Prior to any testing, it was necessary to prepare a solution of the Milling Yellow dye that would display both good birefringent and viscous properties. The solutions were usually prepared by adding 120 grams of Milling Yellow powder to 8,000 grams of distilled water, adding an additional 4,000 grams of distilled water, and boiling the entire batch down to about 8,000 ml (8,000 grams). This method usually provided us with a solution of about 1.4 percent by weight, and exhibited satisfactory birefringent characteristics.

Before installing the fluid in the system, the concentration was checked as accurately as possible, using a 100 gram sample of the solution. This step was found to be very desirable, since the value of the concentration cannot be determined accurately, once the fluid has been circulated through the system. The reason is that the lines and the fittings tend to add contaminants to the fluid, which show up in the concentration analysis.

At first it might appear that this inability to determine the solution concentration would prove to be a problem. However, it is really not necessary to know the value of the concentration, since a fluid calibration can be obtained at any time with the rectangular channel. The only

purpose for obtaining the concentration was to correlate the optic response obtained from the calibration channel with the data published by Peebles, Prados, and Honeycutt[17].

Another step required prior to the actual testing was to calibrate the camera settings and film speed for the amount of light transmitted through the model at a typical flow condition. Photographs were taken of the channel with various f/numbers and shutter speeds. These photographs were evaluated, based on sharpness and clarity of the fringe patterns, and in this manner, we were able to determine the best camera settings. For our original testing, it was found that with the particular film and lens system mentioned previously, an f/2.8 opening at a shutter speed of 1/15 second produced good photographs. It is suggested that this procedure be repeated any time a new flow model is used, or if a change is made from white to monochromatic light.

Finally, it was necessary to calibrate the flowmeters and check the temperature regulation of the mixing valve and heat exchanger. The flowmeters were calibrated with a 2,000 ml graduated cylinder and a stop-watch. Readings were taken for float positions corresponding to the 10, 20, 30, 40, 50, 60, 70 and 100 percent divisions indicated on the tube of the flowmeter. The accuracy of the temperature regulator system was determined by setting a flow rate and recording temperature readings from a thermometer in the model inlet line. It was observed that, for the most part, the regulator functioned fairly well, but intermittant random variations from the mean temperature were observed. For this reason, the fluid temperature was recorded every time a photograph was taken of a particular flow pattern.

It should be mentioned that the flowmeters should be recalibrated every time a new batch of dye is used, and that the calibration will vary somewhat with temperature due to viscosity changes. It is suggested that a complete set of calibration runs be made upon changing the fluid in the system. This will eliminate the problem of recalibration until the fluid is changed again. A reasonable temperature range for calibration data would be from 19°C to 26°C, with data points being recorded for unit temperature increments.

5.2 RECTANGULAR CHANNEL

The first phase of the testing was to determine the correlation between the shear-optic response as obtained from the rectangular

channel with the data published by Peebles, Prados, and Honeycutt[17]. The procedure followed here was to set the temperature of the fluid as closely as possible to 25°C. After the fluid had reached this equilibrium temperature, the flow rate was varied until a reasonable fringe pattern was visible in the 0.25 inch section of the channel. (The 0.25 inch channel section has a 10 to 1 aspect ratio, whereas the 0.50 inch channel section has only a 5 to 1 ratio.) A reasonable fringe pattern was felt to be any pattern having 7 or more distinct equally spaced fringes as shown typically in Figure 5-1. Once such a pattern was obtained, a photograph was taken, using circularly-polarized monochromatic light and the flow rate and the fluid temperature were recorded immediately. This procedure was continued for increasing values of flow until turbulence was observed.

The procedure followed in obtaining the calibration data will now be discussed. A photographic print was selected, which displayed at least seven fringes in the smaller section of the channel, and the data was checked to make sure that the fluid temperature was very close to

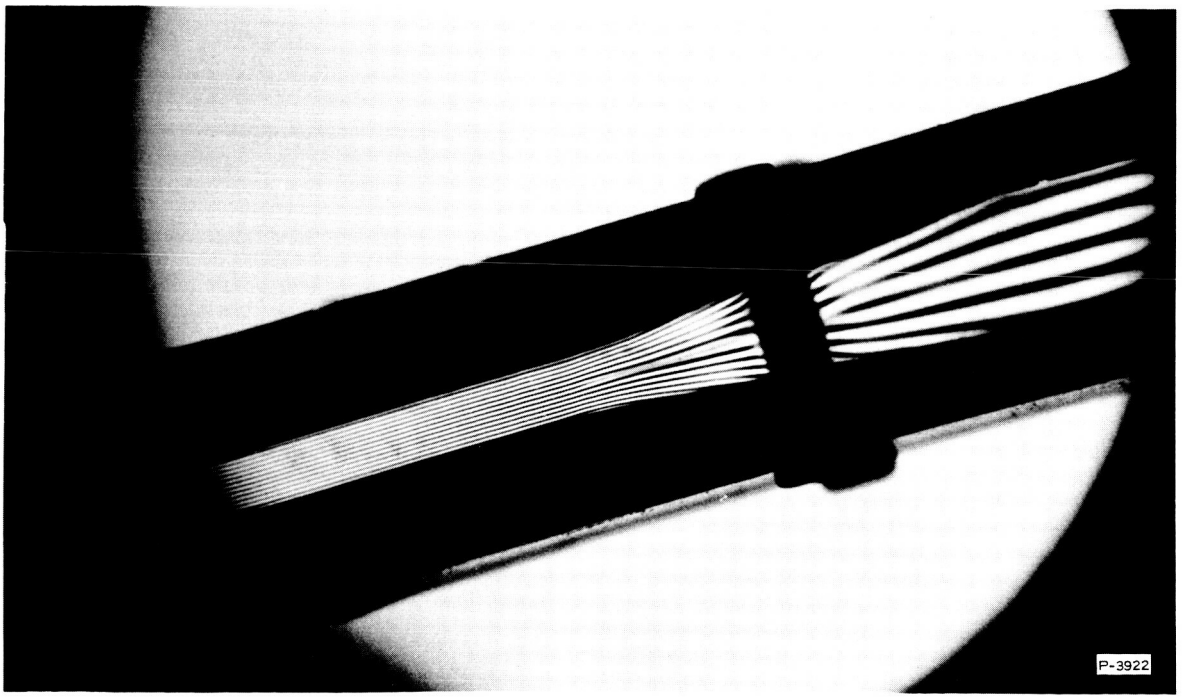

Figure 5-1 - Typical Fringe Pattern in Rectangular Channel

25.0°C. Then the fringe order N was assigned to each fringe in the channel, starting at the channel centerline and working out to both walls. If we equate equations (3.14a) and(3.16)

$$\left| n_e - n_o \right| = \lambda \mu M E_{max} \tag{3.14a}$$

$$\left| n_e - n_o \right| = \frac{N \lambda}{L} \tag{3.16}$$

we obtain

$$N = \mu M E_{max} L \tag{5.1}$$

where

N - fringe order N = 0, 1, 2, ...

μ - fluid viscosity

M - Maxwell constant

E_{max} - maximum rate of deformation

L - optical path distance through the fluid .

From equation(5.1)we see that the fringe order is a monotonically increasing function of the maximum rate of deformation. Assuming constant viscosity, the maximum deformation rate is directly proportional to the distance from the channel centerline, and is equal to zero at the center. Therefore, the fringe at the channel center corresponded to N = 0, the next fringe was N = 1, and so on. From symmetry conditions, this same order had to exist on either side of the centerline. Knowing the order corresponding to each fringe, the birefringence at each point was calculated, using equation (3.16).

It was necessary at this point to determine the maximum rate of deformation at channel positions corresponding to the location of each fringe. These values were computed using equation (3.56).

$$E_{max} = \pm 3 \left(\frac{Q}{A} \right) \frac{y}{h^2} \tag{3.56}$$

These results together with the results obtained using equation (3.16) allowed us to make a plot of birefringence, $n_e - n_o$, versus maximum rate of deformation E.

Since the value of our fluid concentration did not match exactly any of the values for which the published data is available, it was necessary to interpolate these values from the given curves. To do this accurately, a cross-plot of fluid concentration versus birefringence using rate of deformation as a parameter was made for a range of deformation rates. This plot is shown in Figure 5-2(b), and the published data is shown in Figure 5-2(a), where the dashed curve is the result of the interpolation. By locating the value of our concentration on the ordinate in 5-2(b) and extending a horizontal line through this point, the curves of constant rate of deformation are intersected (points x and y). Noting the value of birefringence corresponding to these intersections, we could obtain the plot which is shown dashed in Figure 5-2(a).

The correlation was concluded by superimposing the data points obtained from the analysis of the photographs.

The curves shown in Figure 5-3 show the correlation that was obtained when the shear-optic relation obtained with the rectangular channel of high aspect ratio was compared with the published data in the literature, using fluid concentration as a common denominator. Both curves were obtained for a fluid temperature of 25.0°C. It is evident that the correlation is not close. This result, however, is not indicative of disagreement between the rectangular channel and rotating cylinder polariscope methods of calibration. Milling Yellow dye is a commercial dye and is not prepared on a chemically-pure basis. This is to say,the batch of dye that was used in preparing our test solution would not necessarily contain the same constituents on a percentage basis as that used by Peebles, Prados, and Honeycutt [17]. All data taken with the rectangular channel in the current study have been given birefringence vs deformation rate relationships of a consistent nature, as that shown in Figure 5-3. Based on the foregoing discussion, we conclude that the utilization of a rectangular channel of high aspect ratio to obtain the optic response of a test fluid will provide accurate calibration data.

5.3 VORTEX VALVE

Our next step was to remove the rectangular channel from the optical path and replace it with the fluid state vortex valve model. The convenience of the calibration channel becomes very apparent at this point, since no hydraulic lines must be broken to make this change.

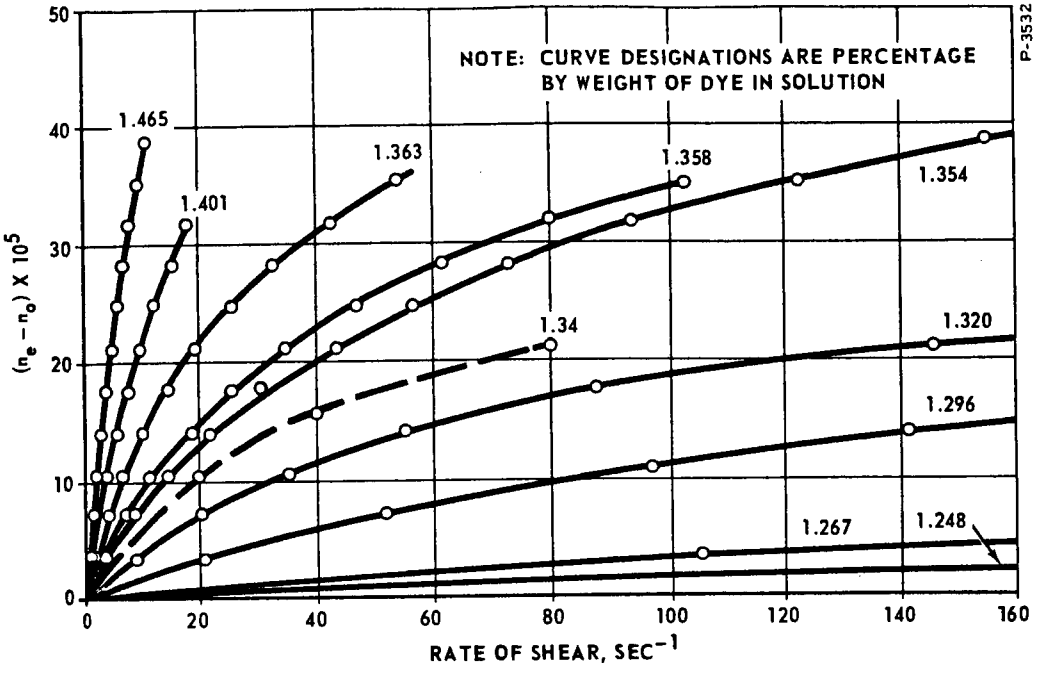

(a) Birefringence Versus Deformation Rate For Concentration Of 1.34 (Shown Dashed) Superimposed On Data Points From Reference 17

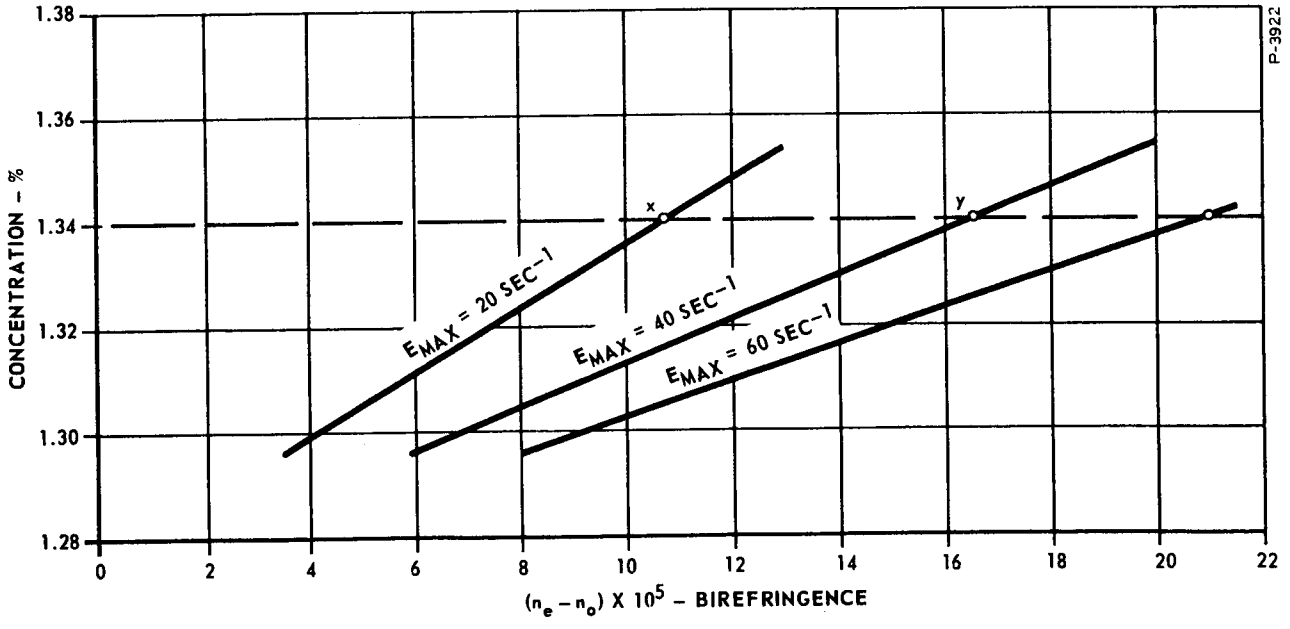

(b) Cross Plot Of Data From Reference 17 Using Deformation Rate As A Parameter

Figure 5-2 - Birefringence, Shear Rate and Concentration Relationships

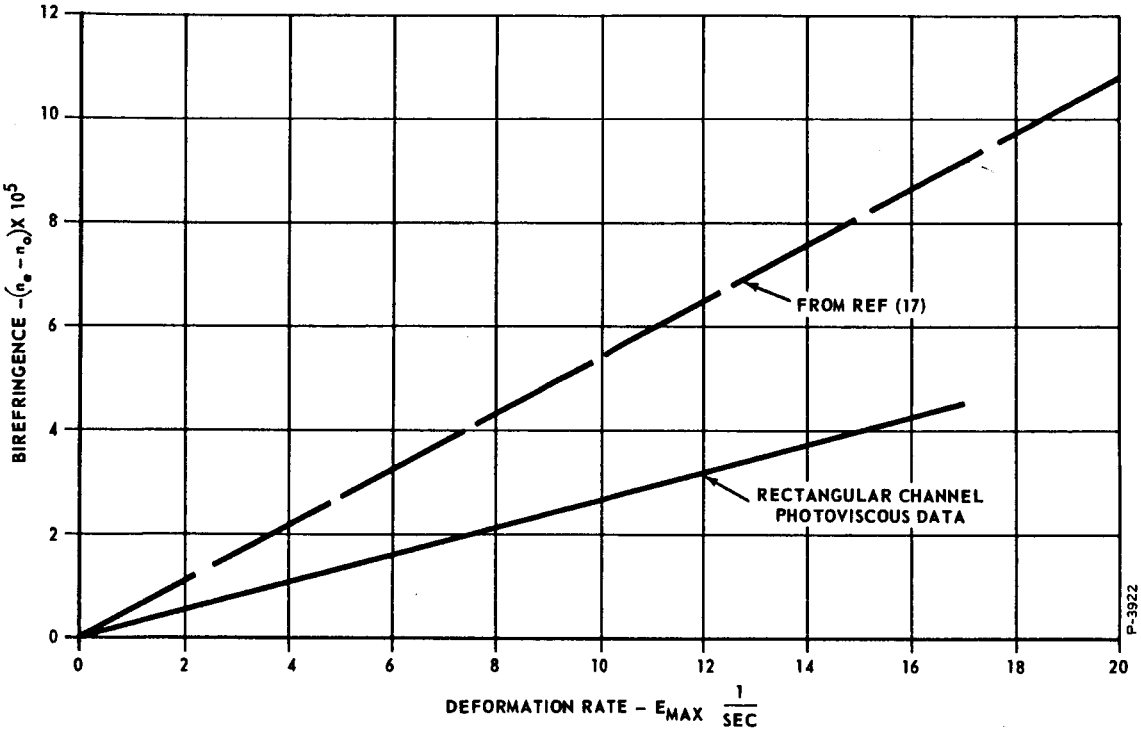

Figure 5-3 - Correlation of Rectangular Channel Data with Published Data

With the vortex valve model in place in the optical path, the flow rate was varied to try to establish a condition where 3 fringes would be visible simultaneously in the field of view. This condition was felt to be necessary, since we were concerned with radial distribution of the fringes, which requires at least three data points. Care was taken to make sure that the order of each fringe was known, precluding the possibility of mistaking the second order fringe for the first, and so on. It was observed that a condition of 3 visible fringes in the vortex field was not obtainable with the fluid at 25°C for flows up to 100 percent. This condition, in fact, was not achieved until the fluid temperature was decreased to 19.0°C, and then occurred only for a flow between 50 and 70 percent. It should be mentioned here that this testing was done with a chamber height in the vortex field of 0.125 inch.

Having determined the conditions necessary to produce the desired fringe patterns, photographs were taken, using circularly-polarized monochromatic light for flow rates ranging from 10 percent to 80 percent. The flow rates and fluid temperatures were recorded with each photograph.

Having obtained all the photographic data from the vortex valve model, it was necessary to put the calibration channel back in the light path and obtain fringe patterns at the same fluid temperature that was used for testing the vortex model. The procedure was the same as indicated previously, with flow and temperature data being recorded for every photograph.

Upon completion of this series of tests, all of the exposed film was processed. For convenience of analysis, 8 in. x 10 in. glossy prints were made of each exposure, which provided us with a 2-to-1 magnification of the actual model size.

The vortex testing was repeated for a chamber height in the vortex field of 0.312 inch. The procedure was exactly the same as indicated previously. The results of both tests will be discussed later in detail.

In obtaining the analytical and experimental correlation of the velocity distribution in the vortex, it was first necessary to determine the relationship between birefringence and maximum rate of deformation for the fluid at 19°C. This was obtained from the photographs of the fringe patterns formed in the calibration channel flowing at 19°C. The procedure in constructing this plot was the same as that indicated previously. From the photographs of the vortex model, we were able to plot the fringe order as a function of radius for a specific flow rate. (This particular photograph contained three visible fringes.) The maximum rate of deformation was obtained for each fringe by first calculating the birefringence $(n_e - n_o)$ for each fringe from equation (3.16), and then using the calibration curve to determine the maximum rate of deformation, E_{max}, corresponding to those calculated values of birefringence. Figure 5-4 shows a typical photograph of the vortex valve for pure radial flow, using circularly polarized monochromatic light.

The velocity distribution occurring in the vortex valve can be obtained entirely from the continuity equation, assuming that the flow is one-dimensional. With this assumption, the continuity equation in cylindrical coordinates becomes

$$\frac{\partial}{\partial r_a} (r_a v_r) = 0 \qquad (5.2)$$

where r_a is the radius and v_r is the radial velocity component. Integration of equation (5.2) with respect to r gives

$$v_r = - \frac{C}{r_a} \qquad (5.3)$$

Figure 5-4 - Vortex Valve, 55 Percent Supply Flow, Zero Control Flow, 18.2°C, Circularly Polarized Monochromatic Light

where C is a constant of integration. The minus sign indicates that the flow is toward the center. Recalling equation (3.39), we have

$$\frac{\partial V}{\partial n} = \frac{V}{r} \pm \sqrt{E_{max}^2 - \frac{4V^2}{r'^2}} \qquad (3.39)$$

where n is the normal to a set of streamlines, r is the radius of curvature of the streamline, r' is the radius of curvature of the normal to a set of streamlines, and E is the maximum rate of deformation. Since in our case the flow in the vortex is purely radial, we have that $\frac{\partial}{\partial n} \equiv \frac{1}{r_a} \frac{\partial}{\partial \theta}$, r is infinite, and r' is equal to r_a. Making these simplifications, we obtain

$$\frac{1}{r_a} \frac{\partial V}{\partial \theta} \equiv 0 = \sqrt{E_{max}^2 - \frac{4v_r^2}{r_a^2}} \qquad (5.4)$$

which can be rewritten as

$$E_{max} = \pm \frac{2 v_r}{r_a} \tag{5.5}$$

Substituting equation (5.3) into (5.5) gives

$$E_{max} = \pm \frac{2 C}{r_a^2} \tag{5.6}$$

From a continuity consideration, we have that the volume flow Q can be expressed as

$$Q = \int_0^{2\pi} r_a v_r h \, d\theta = C h 2\pi \tag{5.7}$$

where h is the chamber height. Rearranging equation (5.7) gives

$$C = \frac{Q}{2 \pi h} \tag{5.8}$$

which when substituted into equation (5.6) gives

$$E_{max} = \frac{Q}{\pi h r_a^2} \tag{5.9}$$

where the positive value has been assumed.

Equation (5.9) was used to determine the theoretical deformation rate distribution. Values of the deformation rate were calculated corresponding to the radial locations of the fringes in the photograph. Sample calculations for obtaining this correlation are shown in Appendix B.

The results of the vortex valve testing are shown in Figure 5-5(a) and 5-5(b). Figure 5-5(a) is for a vortex chamber height of 0.125 inch, and Figure 5-5(b) is for a height of 0.312 inch. It is seen from both Figures that correlation between the analytical and experimental distributions is very poor. It should be noted that the experimental results seem to indicate that the maximum rate of deformation varies with the radial position r_a as

$$E_{max} \propto \frac{1}{r_a^{0.8}} \tag{5.10}$$

This functional relationship is significantly different from that predicted by equation (5.9), which indicates that E varied inversely with the radius

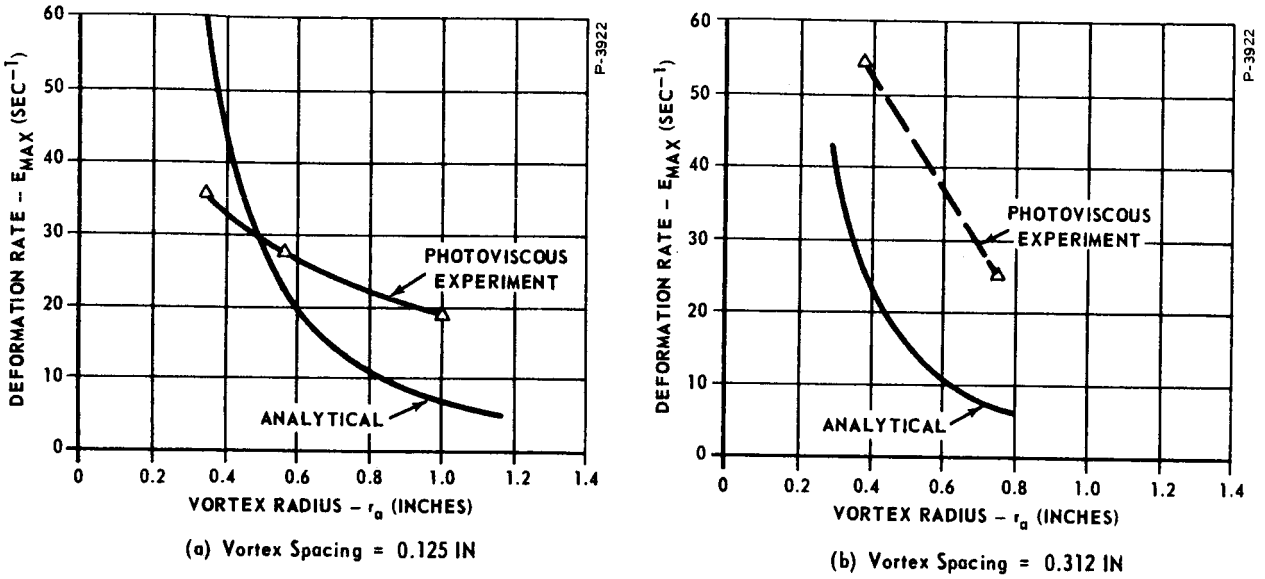

Figure 5-5 - Maximum Deformation Rate Distribution in Vortex Valve for Pure Radial Flow Experimental and Analytical

squared. It is felt that this poor correlation stems from the fact that the aspect ratio in the direction parallel to the light path is much less than unity, which indicates the flow field is essentially three-dimensional. This means that the magnitudes of the stresses in planes perpendicular to the light path are of the same order as in planes parallel to the light path, over most of the vortex chamber height.

In photoelasticity, the stresses in planes perpendicular to the light path have no optical effect. This is a result of the stress-optic law in three dimensions for the photoelastic material. Unfortunately, the stress-optic law in three dimension for birefringent liquids of the Milling Yellow dye type has not yet been established. Our conclusion is that while the quantitative treatment of two-dimensional flow fields by photoviscous techniques can be accomplished, the similar treatment of three-dimensional flow fields are not as yet within the state-of-the-art.

5.4 HIGH SPEED PHOTOGRAPHY

All of the above investigations utilizing the doubly-refracting properties of the Milling Yellow dye solution to obtain quantitative data were confined to the steady-state domain, where the velocity components were functions of coordinate positions only. However, it was determined that quantitative data could be obtained in the transient domain if some high speed photographic techniques were employed.

Our particular investigation was confined to determining the time response of the vortex valve when subjected to a step change in tangential flow. A Hycam Co. high speed movie camera was used in conjunction with a 1,000 watt white light source to record the transient phenomenon. Test runs were made for film speeds of 500, 1,000 and 2,000 frames per second. The control flow line was modified with the addition of a solenoid valve, which was used to provide the step input to the vortex model, in series with the manual valve. The time constant was determined from the processed film by simply running the film slowly through a viewer. By noting the amount of footage required for 63 percentage of the change to occur, and by knowing the film speed, we were able to calculate the time constant. The calculated time obtained by this method compared quite well with analytical predictions.

5.5 QUALITATIVE STUDIES

The use of the photoviscous technique is definitely not limited to investigations of a quantitative nature, but rather is even more powerful in providing qualitative information. Phenomena such as vortex formation, flow instability and laminar-to-turbulent transition can be investigated with photoviscosity.

To employ the photoviscous technique in a qualitative manner, the monostable flip-flop and the vortex valve described previously were tested. The qualitative data was obtained by simply viewing the models with circularly polarized monochromatic light and varying the flow rates through them. Photographs were taken for any flow condition that looked particularly interesting. The qualitative information that was of interest was wall attachment and switching in the flip-flop and noise generation in the vortex valve.

The results of the qualitative testing were very encouraging. Figures 5-6, 5-7, 5-8 and 5-9 are photographs of the monostable flip-flop for increasing values of the supply flow, and from the figures it was deduced that the side wall design was geometrically correct in promoting good wall attachment. Figures 5-10 and 5-11 are photographs of the vortex valve model for two different values of swirl flow. From these photographs, it was concluded that the mixing of the individual tangential jet flows with the supply flow is not confined to the plenum chamber, as had been previously assumed. Rather, the mixing occurs all the way to the outlet hole. In addition, it was concluded that the

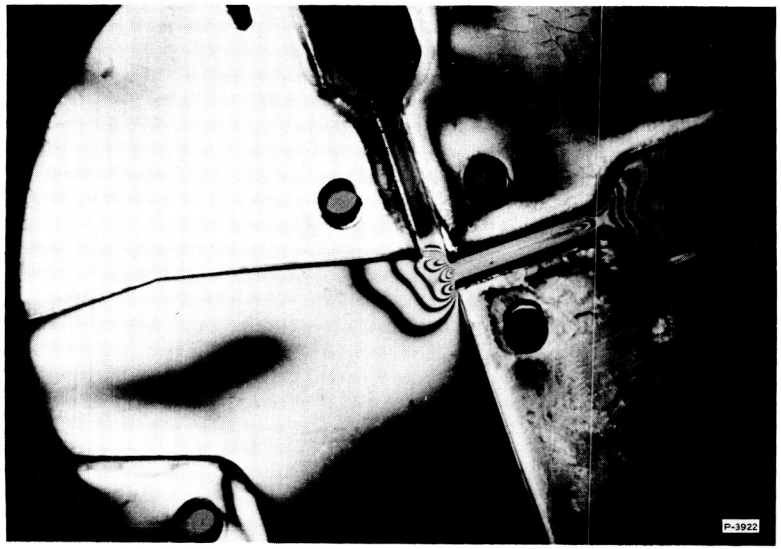

Figure 5-6 - Monostable Flip Flop, 10 Percent Supply Flow, 25°C, Zero Control Flow, Circularly Polarized Monochromatic Light

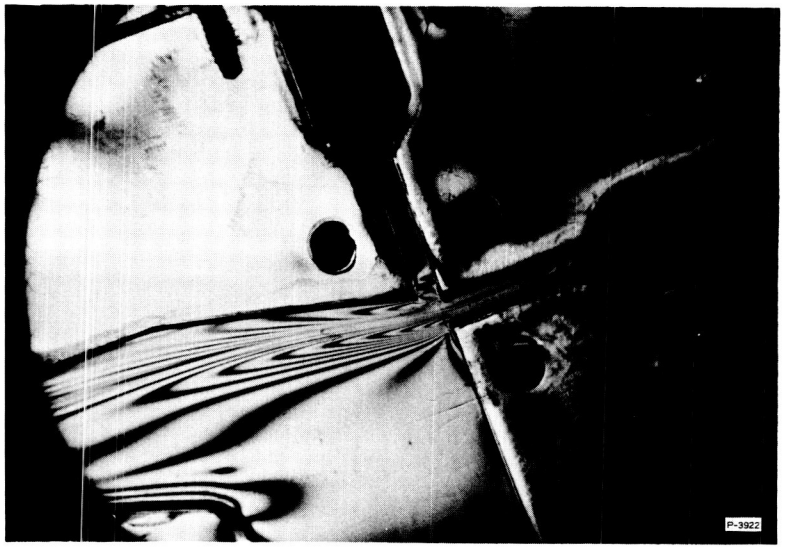

Figure 5-7 - Monostable Flip Flop, 30 Percent Supply Flow, Zero Control Flow, 25°C, Circularly Polarized Monochromatic Light

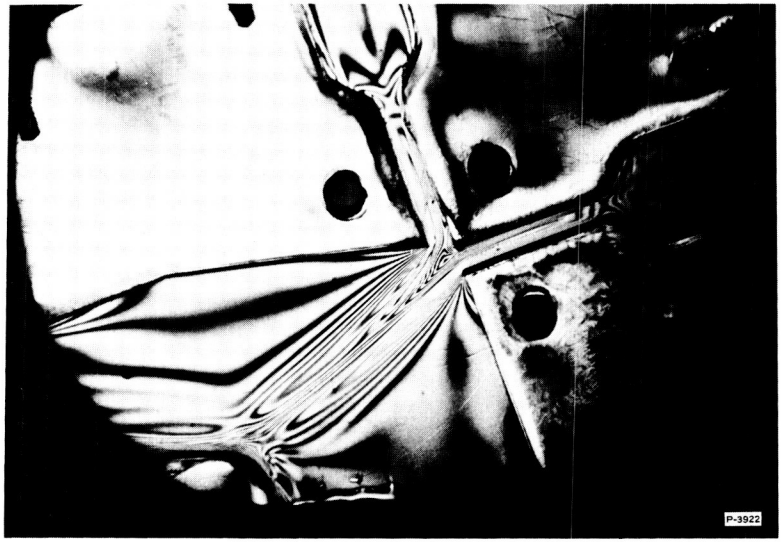

Figure 5-8 - Monostable Flip Flop, 30 Percent Supply Flow, 20 Percent Control Flow, 25°C, Circularly Polarized Monochromatic Light

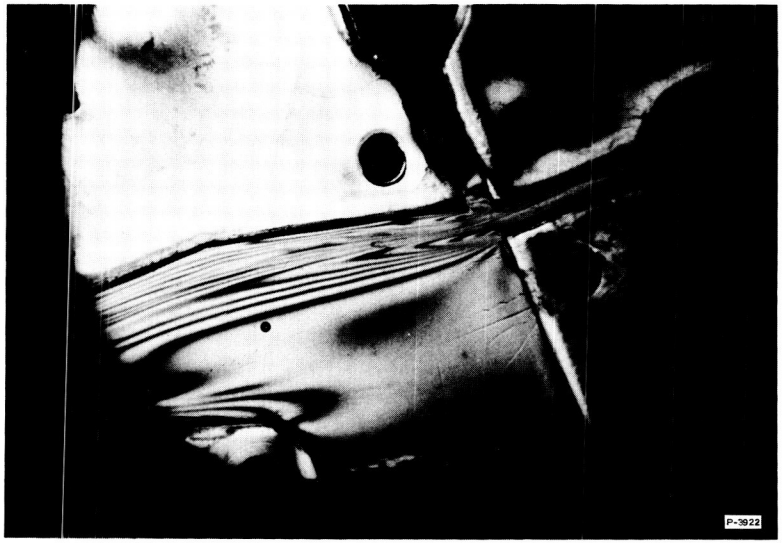

Figure 5-9 - Monostable Flip Flop, 40 Percent Supply Flow, Zero Control Flow, 25°C, Circularly Polarized Monochromatic Light

tangential jets should be located farther upstream from the edge of the button to reduce noise generation. Figure 5-12 shows the mixing pattern obtained after moving the tangential jets further upstream. The photograph was taken using plane-polarized monochromatic light.

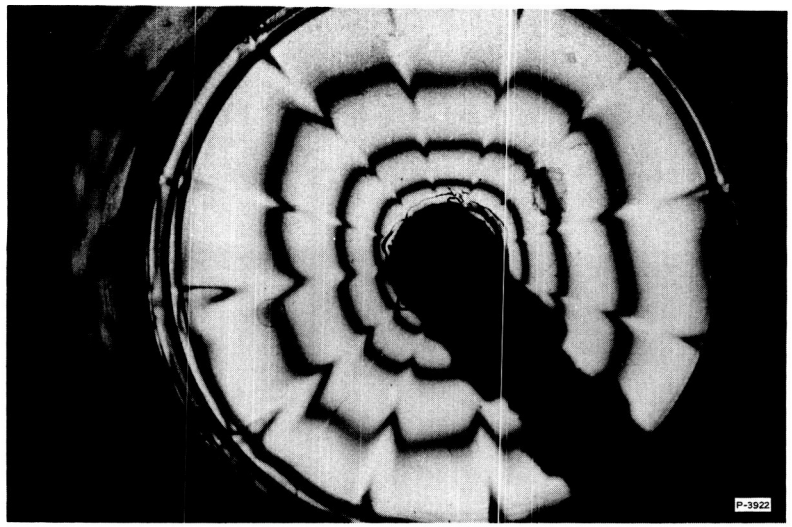

Figure 5-10 - Vortex Valve, 50 Percent Supply Flow, Slight Control Flow, 18.5°C, Circularly Polarized Monochromatic Light

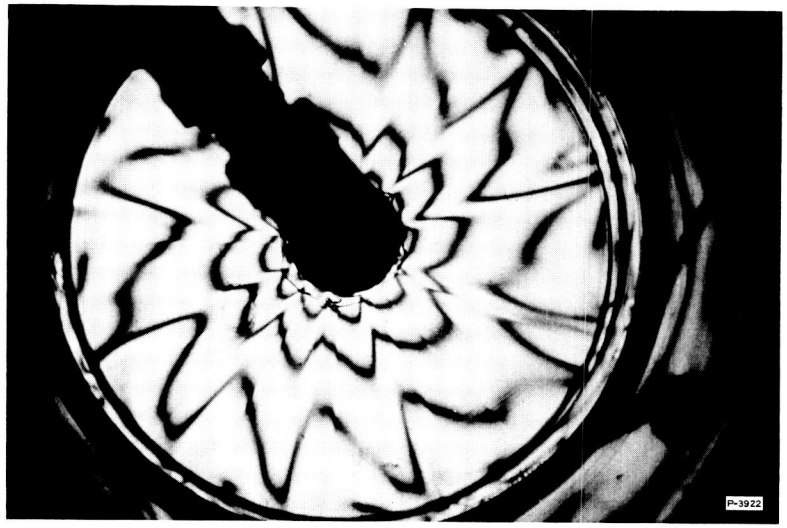

Figure 5-11 - Vortex Valve, 50 Percent Supply Flow, 10 Percent Control Flow, 18.5°C, Circularly Polarized Monochromatic Light

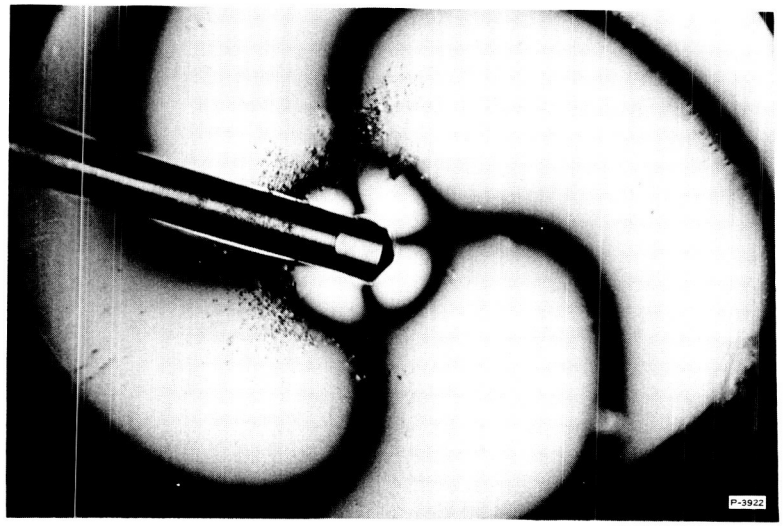

Figure 5-12 - Redesigned Vortex Valve, Zero Supply Flow, 40 Percent Control Flow, 18.0°C, Plane Polarized Monochromatic Light

SECTION 6

CONCLUSIONS AND RECOMMENDATIONS

Based on the work that has been performed, the following conclusions have been reached:

(1) The equipment which has been developed provides a convenient and useful means for examining a variety of fluid flow fields geometries.

(2) The calibration channel approach described in Section 5.2 has many advantages over the rotating cylinder polariscope for conveniently calibrating the photoviscous liquid being used. The calibration procedure obtains the birefringence vs deformation rate relationship for the liquid at a given temperature.

(3) At present, quantitative information on the fluid velocity field in a model (streamline pattern) can be obtained only where three-dimensional effects are not significant. The limitation to two-dimensional flow fields is a consequence of incomplete knowledge of the stress-optic law for Milling Yellow dye solutions. The limitation is illustrated by the lack of correlation between observed and predicted fringe patterns in the vortex valve experiments described in Section 5.3. Amplification of the two-dimensional flow criterion will be given below.

(4) Existing methods [20] allow numerical computation of the velocity field in two-dimensional flow, using the isochromatic fringe pattern. Of course, the flow must not be turbulent. Also, the shear rates in the fluid must not exceed the point where the viscosity becomes variable, if the flow in the model is to represent that of a constant-viscosity fluid. Another reason for staying in the constant-viscosity range for the photoviscous fluid is to avoid inaccuracies caused by different optic responses to gliding and dilation shear deformations.

(5) The measurement of internal dynamic response times in fluid flow components can be accomplished by using high speed motion picture photography in conjunction with photoviscous flow visualization. This is potentially a very useful experimental method.

(6) Qualitative information can be obtained readily by the photoviscous technique, even when the flow field is three-dimensional. Such information includes the observation of flow instabilities, Coanda effects, vortex formation, and the transition between laminar and turbulent flow regimes. The qualitative application of photoviscosity offers promise as a method for diagnosing performance difficulties in fluid flow components and for guiding design modifications.

In (3) above, the criterion of two-dimensional flow was stated in connection with quantitative determination of a flow field from photoviscous data. A confined flow is considered two-dimensional if the aspect ratio of the flow geometry is large. Figure 6-1(a) illustrates a flow geometry where the aspect ratio, defined as L/h, is less than unity. Over most of the light path through the fluid, the shear rates in planes perpendicular to the light direction are of the same magnitude or greater than the shear rates in planes parallel to the light direction. This is a three-dimensional flow geometry.

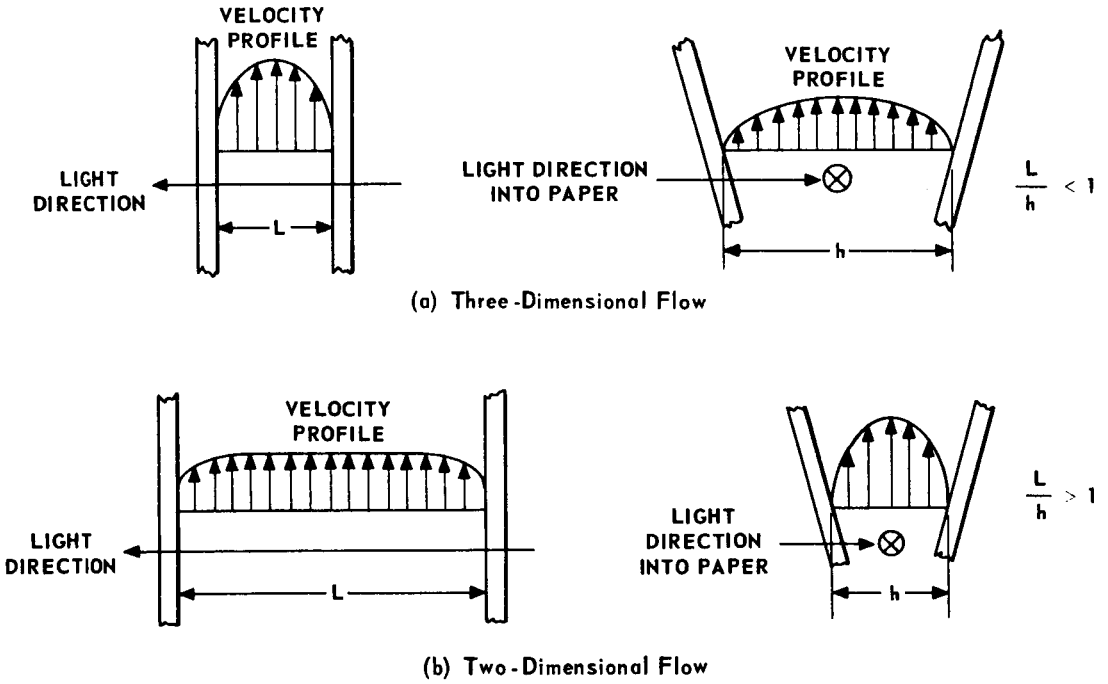

Figure 6-1 - Aspect Ratio of Flow Passage

Figure 6-1(b) illustrates a case where the aspect ratio L/h is larger than unity. Over most of the light path, the shear rates in planes perpendicular to light direction are negligible, compared with the shear rates in planes parallel to the light direction. This is a two-dimensional flow geometry. As a rule-of-thumb, the aspect ratio should be at least 5, or preferably 10 or greater, to ensure a two-dimensional flow. The practical significance of the aspect ratio criterion, regarding quantitative analysis of the flow field in fluid state devices, is illustrated in Figure 6-2. The distance L is at least 5 times greater than the largest dimension D_m of the amplifier contour.

Our recommendations concerning the photoviscous technique are as follows:

(1) The equipment developed should be put into use for studying the flow fields in fluid flow components of interest, particularly in fluid state devices.

(2) Where the aspect ratio criterion for two-dimensional flow is met by the model, quantitative determinations of the viscous stress and streamline patterns should be made.[20] Otherwise, qualitative observations should be made, such as those relating to noise generation in fluid state amplifiers.

(3) Specific attention should be given to using high speed motion picture photography in conjunction with the photoviscous test equipment, since this appears to be a uniquely advantageous method of measuring internal response times in fluid state devices.

(4) The rectangular channel method of calibrating photoviscous fluid should be used in conjunction with the test equipment developed.

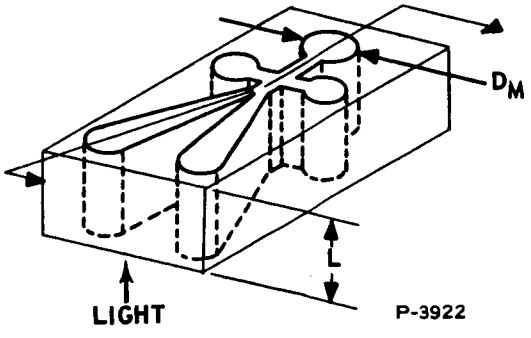

Figure 6-2 - Device Model with Large Aspect Ratio

(5) Rheological measurements should be added to the photoviscous fluid calibration procedure. This might be accomplished by a capillary passage permanently installed on the test stand, and capable of being valved into the fluid circulation system when required. The differential pressure across the capillary passage would be measured by a manometer, and the viscosity calculated from the flow rate and differential pressure data. The determination of fluid viscosity will permit the accurate modeling of experiments according to Reynolds number, and the checking of the Newtonian shear rate range of the fluid.

(6) Further study should be done to determine the stress-optic law in three dimensions for Milling Yellow dye solution. The objective should be the extension of present quantitative methods to flow geometries having small aspect ratios.

LIST OF REFERENCES

1. Alcock, E. D. and C. L. Saldron, Physics 6, 92 (1935).
2. Binnie, A. M. "A Double Refraction Method of Detecting Turbulence in Liquids", Proceedings of the Physical Society (London) 57, 390-402, (1945).
3. Boeder, P. Z., Physik 75, 258 (1932).
4. Dewey, D. R., PhD., Dissertation, Massachusetts Institute of Technology, Cambridge (1941).
5. Frocht, M. M., Photoelasticity, Vol. I, John Wiley, New York (1941).
6. Hauser, E. A. and D. R. Dewey, Industrial Engineering Chemistry, 31, 786 (1939).
7. Hauser, E. A., Journal of Physical Chemistry, 46, 212 (1942).
8. Hirsch, A. E., "The Flow of a Non-Newtonian Fluid in a Diverging Duct, Experimental," PhD. Dissertation, University of Tennessee (1964).
9. Humphry, R. H., Proceedings of the Physical Society, (London) 35, 217 (1923).
10. Jeffery, G. B., "The Motion of Ellipsoidal Particles Immersed in a Fluid", Proceedings of the Royal Society, (London/Series A, Vol. 102) 161 (1923).
11. Jessop, H. T. and F. C. Harris, Photoelasticity, Principles and Methods, Dover, New York, (1950).
12. Leaf, W. "Fluid Flow Study of Locomotive Fire Box Design", Mechanical Engineering, 67, 586-590 (1945).
13. Lindgren, E. R., Arkin Fysik, 7, 293 (1954).
14. Maxwell, J. C., Proceedings of the Royal Society (London) 22, 46 (1873).
15. Peebles, F. N., H. J. Garber and S. M. Jury, Preliminary Studies of Flow Fluid Mechanics, University of Minnesota Press (1953).

16. Peebles, F. N. and K. C. Liu, "Photoviscous Analysis of Two-Dimensional Laminar Flow in an Expanding Jet", Experimental Mechanics, September 1965.

17 Peebles, F. N., J. W. Prados, E. H. Honeycutt, Jr., Journal of Polymer Science, Part C, No. 5, p. 37.

18. Prados, J. W., "The Analysis of Two-Dimensional Laminar Flow Utilizing a Doubly Refracting Liquid", PhD., Dissertation, University of Tennessee (1957).

19. Roshenow, W. M. and H. Y. Choi, Heat, Mass and Momentum Transfer, Prentice-Hall, Englewood Cliffs, p. 45 (1961).

20. Rosenberg, B., Report 617, Navy Dept., David W. Taylor Model Basin, Washington 7, D.C. (1952).

21. Thurston, G. B., and L. E. Hargrove, "Optical Birefringence Induced by Shear Wave Propagation in Aqueous Milling Yellow Solutions", Reports 1 and 4, AD-134-151.

LIST OF SYMBOLS

Symbol		Meaning
a	=	"Breakpoint" shear rate
A	=	Light vector amplitude; Diaphragm area
A_v	=	Valve area
b	=	Dimensionless number
C	=	Wavelength; Constant
C_p	=	Specific heat at constant pressure
E	=	Deformation rate
f	=	Functional notation
F	=	Force
F'	=	Component of light ray vector along optic axis
h	=	Channel half height; Vortex spacing
L	=	Optical path thickness in the fluid
L/h	=	Aspect ratio
M	=	Maxwell constant
n	=	Normal to a set of streamlines; Index of refraction
N	=	Fringe order
p	=	Hydrostatic pressure
ΔP	=	Pressure drop across valve
Q	=	Volume flow rate; Heat flow
r	=	Radius of curvature of streamline
r'	=	Radius of curvature of normal curve to a set of streamlines
r_1, r_2	=	Inner and outer radii of Polariscope
r_a	=	Geometric radius in vortex valve
R	=	Resultant ray vector at analyzer

Symbol		Meaning
S	=	Streamline
S'	=	Component of light ray vector along optic axis
t	=	Time
T	=	Temperature
u	=	Amplitude of light vector at any time; Velocity in x direction
$\bar{u}$	=	Average velocity
U_o	=	Velocity along channel centerline
v	=	Velocity in y direction
V	=	Velocity along streamline
w	=	Velocity in z direction
x	=	Valve travel
x_d	=	Development length in channel
x, y, z	=	Position coordinates
β	=	Angle between the polarizer axis and the local optic axis in the fluid
∂	=	Partial derivative symbol
δ	=	Relative retardation (phase shift)
θ	=	Angle formed by deformation rate with x axis
λ	=	Wavelength
μ	=	Absolute viscosity
ν	=	Kinematic viscosity
ξ	=	Arbitrary angle with respect to x axis
π	=	Constant (3.1416..)
σ	=	Normal stress
τ	=	Shear stress
ϕ	=	Angle formed by streamline with the x axis

Symbol	Meaning
χ	Extinction angle
ψ	Stokes stream function
ω	Angular frequency; Frequency of light ray vector

Symbol Subscripts	Meaning
e	Extraordinary
o	Ordinary

APPENDIX A

SHEAR-OPTIC CALIBRATION CURVE

In Section 5.2, the procedure for obtaining the shear-optic relation for a photoviscous liquid was indicated. This Appendix will demonstrate the procedure with actual calculations, using the fringe pattern shown in Figure A-1 as an example. The photograph was taken using circularly-polarized monochromatic light. (Sodium vapor light source; $\lambda = 2.32 \times 10^{-5}$ inches). The volume flow rate through the channel was 1.46 cubic inches per second.

The fringe orders and their locations as measured on the photograph are shown in Table A-1. The actual distances of the fringes from the channel centerline are given in the next column. The actual distance is equal to the distance on the photograph divided by the print magnification factor. (This factor is obtained by measuring the spacing of the smaller channel section on the photograph, which is actually 0.25 inch.)

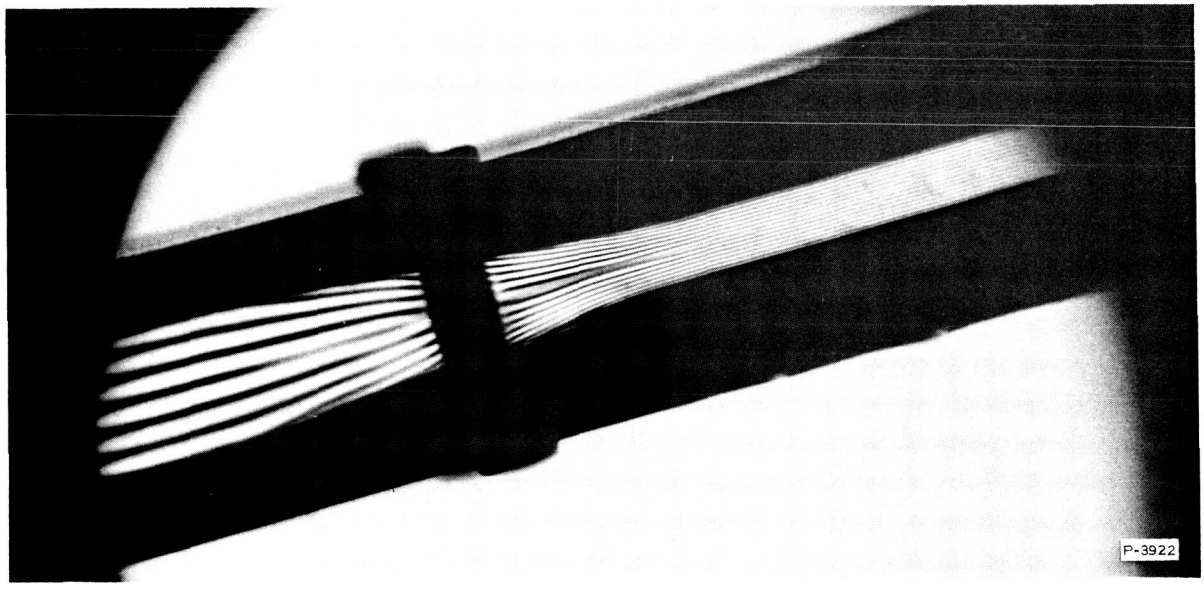

Figure A-1 - Calibration Channel, 1.46 in^3/sec Flow Rate, 25.0°C, Circularly Polarized Monochromatic Light

Table A-1 - Fringe Orders and Their Locations

Fringe Order	Distance From Centerline (Photo) (inches)	Actual Distance (inches)	Birefringence $(n_e - n_o) \times 10^5$	Deformation Rate E_{max} (sec^{-1})
0	0	0	0	0
1	0.030	0.0167	0.927	7.48
2	0.060	0.0334	1.85	14.50
3	0.090	0.05	2.78	22.40
4	0.120	0.066	3.71	29.65
5	0.150	0.083	4.64	37.20
6	0.180	0.10	5.56	44.80
7	0.210	0.1167	6.48	52.10

P-3922

In the next column is the birefringence corresponding to each fringe. The numerical value is obtained from equation (3.16)

$$\left|n_e - n_o\right| = \frac{N\lambda}{L} \qquad (3.16)$$

where

L - optical path thickness; 2.5 inches

λ - wavelength; 2.32×10^{-5} inches for sodium vapor

N - fringe order; (0 to 7)

for this case. Substituting the values for λ and L into equation (3.16)

$$(n_e - n_o) \times 10^5 = 0.927\ N \ .$$

The last column gives the value of the deformation rate existing in the fluid at the positions corresponding to each of the fringe locations. The values are calculated from equation (3.56) which gives

$$E_{max} = \pm 3 \left|\frac{Q}{A}\right| \frac{y}{h^2} \qquad (3.56)$$

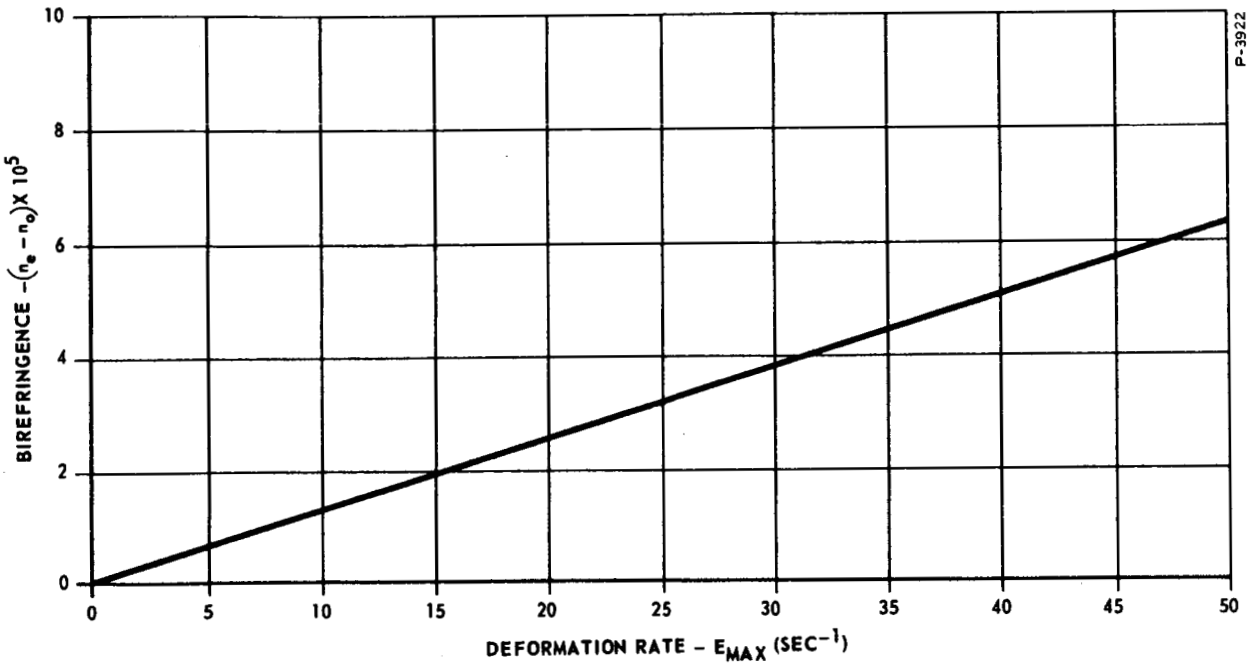

Figure A-2 - Birefringence Versus Deformation Rate for Figure B-1

where

Q - volume flow rate; 1.46 in^3/sec

A - cross-section area of the channel; 0.625 in^2 (0.25 x 2.5)

y - actual fringe location; variable

h^2 - channel half-height; $(0.125)^2 = 0.015625\ in^2$

Substituting these numerical values into equation (3.56) gives

$$E_{max} = 448\ y$$

where y takes on the values indicated in the column entitled "Actual Distance". The resultant plot is shown in Figure A-2.

APPENDIX B

VORTEX VALVE CORRELATION

This Appendix demonstrates the procedure described in Section 5.3 for determining the correlation between photoviscous experimental and fluid mechanics theoretical results. The case for which the correlation is examined is a vortex valve with only radial flow.

In Figure B-1 is shown a photograph of the vortex valve taken with circularly polarized monochromatic light. The supply flow through the valve was 2.76 cubic inches per second, and the fluid temperature was 18.2°C. No control (swirl) flow was present.

Figure B-1 - Vortex Valve, 50 Percent Supply Flow, Zero Control Flow, 18.2°C, Circularly Polarized Monochromatic Light

The photograph shows three radial fringes present in the valve, and from other photographs of the same valve for lower flow rates, it was determined that these three fringes are the second, third and fourth order fringes. The second fringe is located at the outer edge of the valve, while the fourth fringe is just outside the outlet fitting. The axial spacing of the walls of the vortex valve in this photograph is 0.125 inch, and the light source used was a sodium vapor lamp.

The values of the maximum rate of deformation corresponding to each of these fringes were obtained from a calibration curve of the fluid, obtained by flowing the rectangular channel at the same fluid temperature and taking photographs of the fringe patterns produced at various flow rates. A typical photograph of the flow channel is shown in Figure B-2. The flow rate through the channel was 1.433 cubic inches per second, and this photograph was also taken using circularly polarized sodium vapor light. The calibration curve was obtained following a procedure identical with that shown in Appendix A. The fluid calibration at 18.2°C is shown in Figure B-3.

The value of the deformation rate corresponding to each fringe in the vortex model is obtained by computing the amount of birefringence corresponding to the fringe from

$$\left| n_e - n_o \right| = \frac{N\lambda}{L} \qquad (3.16)$$

where

λ = wavelength of sodium vapor light; 2.32×10^{-5} inches

L = optical path thickness; 0.125 inch

Substituting these values gives

$$\left| n_e - n_o \right| \times 10^5 = 18.5\ N\ .$$

In Table B-1, the values of the deformation rates are taken from an extrapolated curve of Figure B-3, since the maximum birefringence obtained with the calibration channel was less than the minimum birefringence existing in the vortex valve. (It was thought that this necessary extrapolation was introducing a large error in the correlation, but when the birefringence in the vortex was reduced by increasing the optical path thickness, no significant change in the correlation of experimental and theoretical results was seen.)

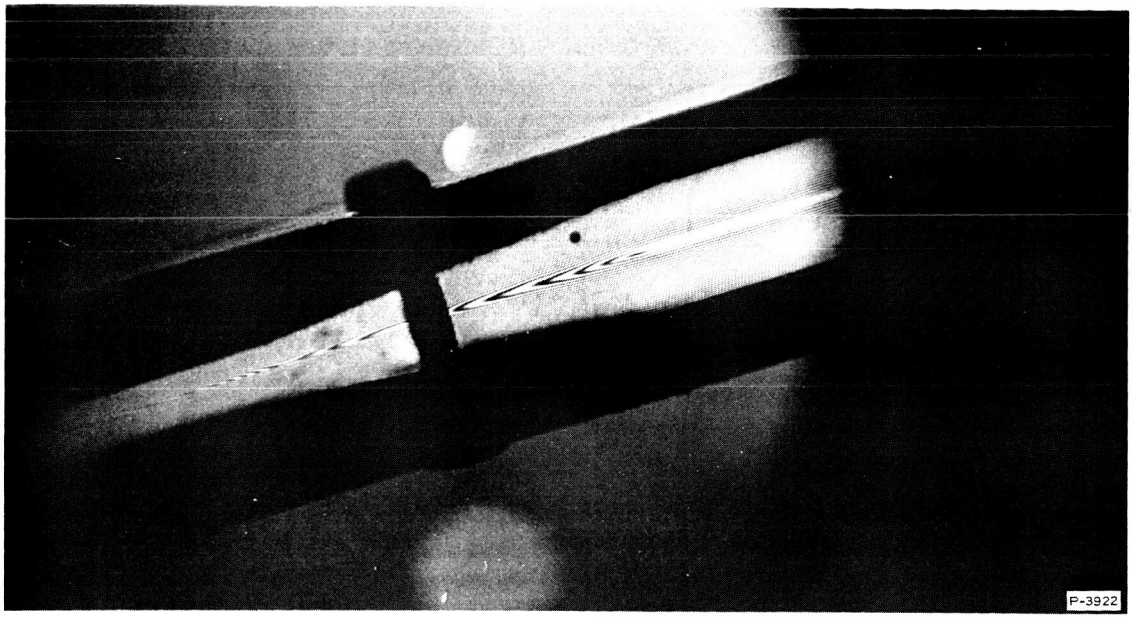

Figure B-2 - Calibration Channel, 1.433 in^3/sec Flow Rate, 18.2°C, Circularly Polarized Monochromatic Light

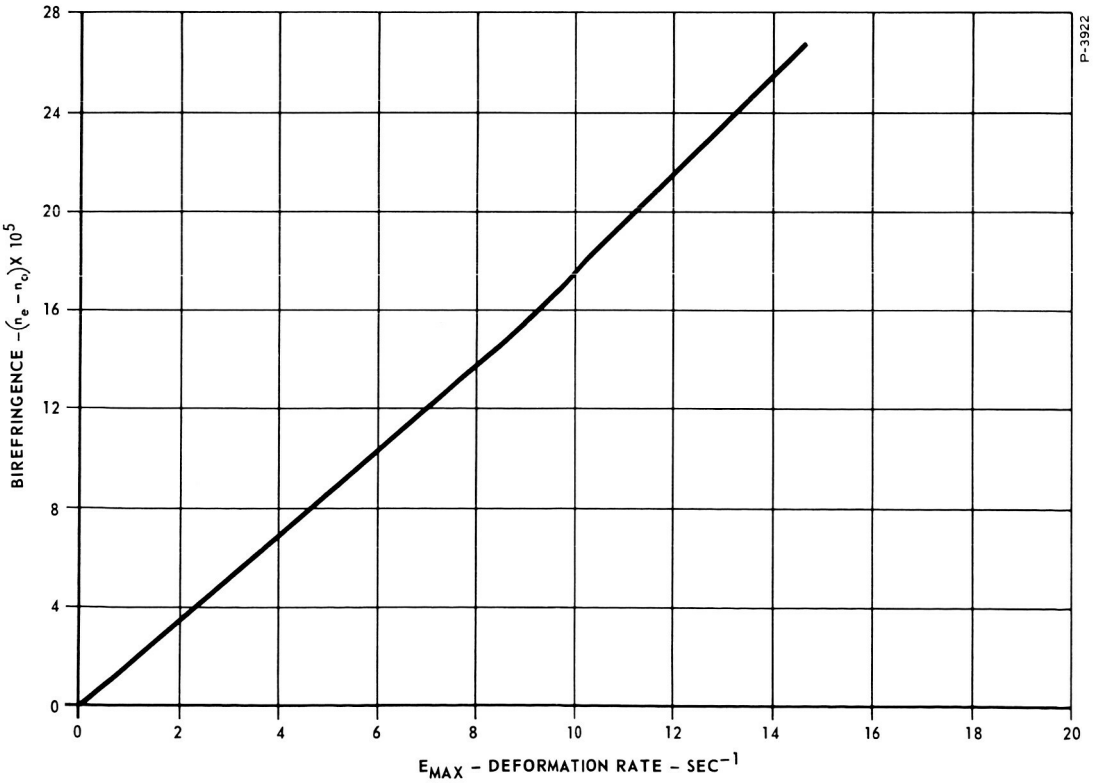

Figure B-3 - Shear-Optic Response for Test Fluid at 18.2°C

Table B-1 - Values of Deformation Rates

Fringe Order	Photo Radius	Actual Radius	Birefringence $(n_e - n_o) \times 10^5$	E_{max} From Figure B-3	E_{max} Calculated
2	2.4	1.00	37.0	19	7.04
3	1.35	0.56	55.5	27.5	22.4
4	0.8	0.334	74.0	36.0	63.1

P-3922

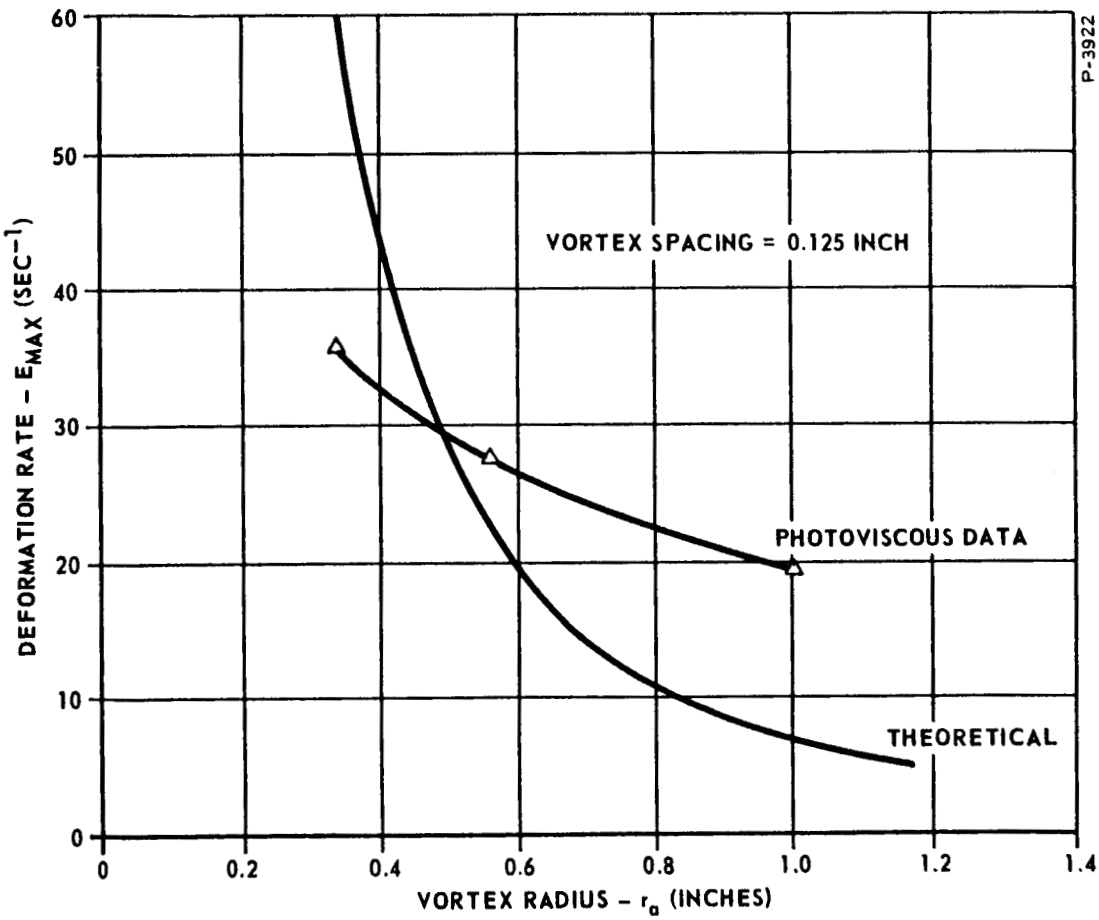

Figure B-4 - Maximum Deformation Rate Distribution in Vortex Valve for Pure Radial Flow - Experimental and Analytical

The columns entitled "Photo Radius" and "Actual Radius" correspond to the radial position of the fringes as indicated by the photograph and the actual position of the fringe when the scale factor of the print is taken into account. (The outer diameter of the valve is 3.00 inches.)

The theoretical deformation rates are calculated from equation (5.9), which gives

$$E_{max} = \frac{Q}{\pi r_a^2 h} \qquad (5.9)$$

where

Q = volume flow rate; 2.76 cubic inches per second

h = spacing in the vortex valve; 0.125 inch (also equal to L, the optical path thickness)

r_a = radius; inches

Substituting these numerical values into the above expression we obtain

$$E_{max} = \frac{7.04}{r_a^2}$$

The values of r_a used for calculation correspond to the radial positions of the three fringes. The resultant plot is shown in Figure B-4.

APPENDIX C

FLOW OF A NON-NEWTONIAN FLUID IN A RECTANGULAR CHANNEL OF HIGH ASPECT RATIO

The non-Newtonian behavior of Milling Yellow dye photoviscous fluid has been described by Peebles, Prados and Honeycutt[17]. Figure C-1 is a plot of the data given in Reference 1. Up to a point the viscosity is constant, and then it drops off with increasing shear rate. We will consider only the constant viscosity range and the range where the viscosity is falling. That is, we will not consider the range where the viscosity is asymptotically approaching a new constant value.

With this simplification, we will approximate the viscosity vs. shear rate relationship by two straight lines. The first one is horizontal

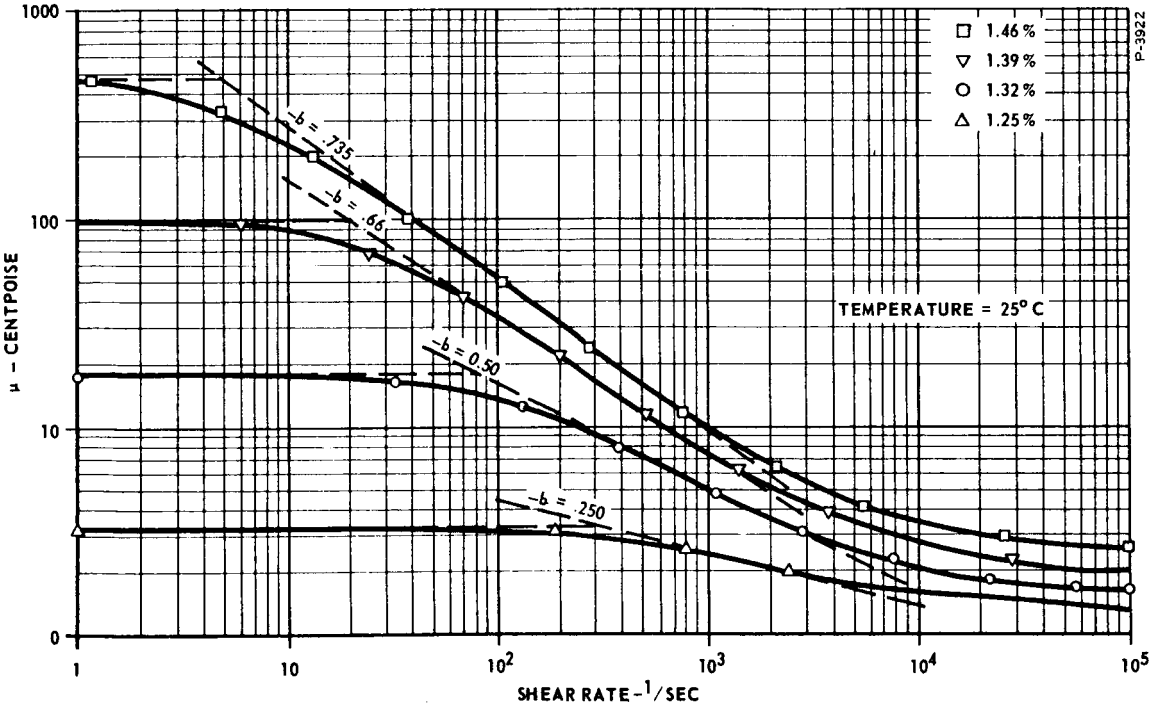

Figure C-1 - Variation of Viscosity with Shear Rate for Various Concentrations of Milling Yellow Dye (From Reference 17)

and indicates the Newtonian, constant viscosity region, and the shear rate at the end of this region is denoted by a. The second line has a slope - b and passes through a. Since this is a log-log plot, the equation relating viscosity and shear rate in this region is:

$$\mu = \mu_o \left[\frac{-a}{\frac{\partial u}{\partial y}} \right]^b \qquad (1)$$

where

μ = viscosity, centipoise

μ_o = viscosity in the low shear rate region, centipoise

$-a$ = "break point" shear rate, sec^{-1}

b = dimensionless number

$\frac{\partial u}{\partial y}$ = shear rate, sec^{-1}

The quantities a and b are constants for a given solution concentration.

Figure C-2 shows a cross-section of a parallel wall channel of unit depth. The axis lies along the center line of the channel and the y axis is perpendicular to the centerline. The half height of the channel is h. Assuming no velocity in the y direction and a pressure gradient in the x-direction, the Navier-Stokes equation reduces to the familiar form

$$\frac{\partial p}{\partial x} = \frac{\partial}{\partial y} \left[\mu \frac{\partial u}{\partial y} \right] \qquad (2)$$

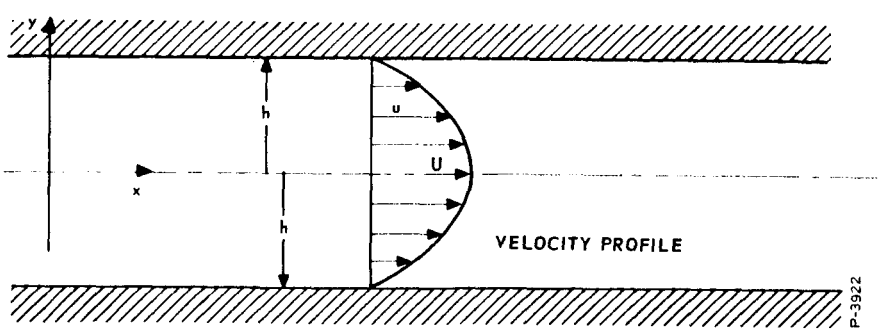

Figure C-2 - Channel Coordinate System

where

p = pressure

x = distance along length of channel

y = distance perpendicular to channel walls

u = velocity in x-direction

μ = absolute viscosity

The flow is thought of as two distinct parts; one, Newtonian, and the second, non-Newtonian. At the centerline, the shear rate is zero, so the flow is Newtonian; from there, the Newtonian region extends out to the point where $\frac{\partial u}{\partial Y} = -a$, then from this point to the wall, the flow is non-Newtonian and the viscosity obeys the law

$$\mu = \mu_o \left[- \frac{a}{\frac{\partial u}{\partial Y}} \right]^b \qquad (3)$$

as in (1) above

In the Newtonian range $\mu = \mu_o$ = constant, and equation (2) becomes

$$\frac{\partial p}{\partial x} = \mu_o \frac{\partial^2 u}{\partial y^2} \qquad (4)$$

In the non-Newtonian range equation (3) is substituted into equation (2) resulting in

$$\frac{\partial p}{\partial x} = \mu_o (-a)^b \frac{\partial}{\partial y} \left[\left(\frac{\partial u}{\partial y} \right)^{1-b} \right] \qquad (5)$$

The boundary conditions are:

at $y = 0$, $\frac{\partial u}{\partial y} = 0$

at $y = \pm h$, $u = 0$.

where

h = half-height of channel

The matching conditions at the boundary between the Newtonian and non-Newtonian regions are

$$y = y_a, \quad \frac{\partial u}{\partial y} = -a, \quad u = u_a$$

Equation (4) can be integrated directly to get $\frac{\partial u}{\partial y}$ and u as:

$$\left.\begin{aligned} \frac{\partial u}{\partial y} &= \frac{1}{\mu_o} \frac{dp}{dx} y + C_1 \qquad (6) \\ u &= \frac{1}{2\mu_o} \frac{dp}{dx} y^2 + C_1 y + C_2 \qquad (7) \end{aligned}\right\} 0 \le y \le y_a$$

Integrating equation (5) once gives

$$\left(\frac{\partial u}{\partial y}\right)^{1-b} = \frac{y}{\mu_o (-a)^b} \frac{dp}{dx} + C_3 \quad . \qquad (8)$$

It is convenient here to eliminate C_3 by using equation (6) and the matching condition of $\frac{\partial u}{\partial y} = -a$ at $y = y_a$. Since $\frac{\partial u}{\partial y} = 0$ at $y = 0$, $C_1 = 0$. Therefore,

$$\frac{\partial u}{\partial y} = \frac{1}{\mu_o} \frac{dp}{dx} y \quad . \qquad (9)$$

The matching condition gives

$$y_a = \frac{-a\mu_o}{\frac{dp}{dx}} \qquad (10)$$

Substituting equation (10) into equation (8):

$$(-a)^{1-b} = \frac{-a\mu_o}{\frac{dp}{dx}} : \frac{\frac{dp}{dx}}{\mu_o (-a)^b} + C_3$$

or

$$(-a)^{1-b} = (-a)^{1-b} + C_3$$

This last equation shows that $C_3 = 0$ for all values of b. Therefore equation (8) is simplified to

$$\frac{\partial u}{\partial y} = \left[\frac{y}{\mu_o (-a)^b} \quad \frac{dp}{dx} \right]^{\frac{1}{1-b}} \tag{11}$$

Integration of equation (11) produces

$$u = \left[\frac{1}{\mu_o (-a)^b} \quad \frac{dp}{dx} \right]^{\frac{1}{1-b}} \left(y^{\frac{2-b}{1-b}} \right) \frac{1-b}{2-b} + C_4 \quad .$$

Using $u = 0$ at $y = h$, C_4 can be evaluated to leave

$$u = \frac{1-b}{2-b} \left[\frac{h}{\mu_o (-a)^b} \quad \frac{dp}{dx} \right]^{\frac{1}{1-b}} h \left[\left(\frac{y}{h} \right)^{\frac{2-b}{1-b}} - 1 \right] . \tag{12}$$

At this point, we will make the following definition:

$$P = \frac{-h \frac{dp}{dx}}{\mu_o a} \tag{13}$$

This non-dimensional quantity, P, is the ratio of the pressure forces to the shearing forces. Equation (12) now becomes

$$\frac{u}{ah} = - \left(\frac{1-b}{2-b} \right) \left(P^{\frac{1}{1-b}} \right) \left[\left(\frac{y}{h} \right)^{\frac{2-b}{1-b}} - 1 \right] , \quad \frac{1}{P} < \frac{y}{h} < 1 . \tag{14}$$

C_2 is evaluated from equations (7) and (14) by using the velocity matching condition, $u = u_a$ at $y = y_a$. From equation (14),

$$\frac{u_a}{ah} = - \left(\frac{1-b}{2-b} \right) \left[P^{\frac{1}{1-b}} \right] \left[\left(\frac{1}{P} \right)^{\frac{2-b}{1-b}} - 1 \right] . \tag{15}$$

From equation (7)

$$\frac{u_a}{ah} = - \frac{1}{2P} + \frac{C_2}{a h} . \tag{16}$$

Solving these for $\frac{C_2}{ah}$ gives

$$\frac{C_2}{ah} = \frac{1}{2P}\left(\frac{b}{2-b}\right) + \frac{1-b}{2-b}\,P^{\frac{1}{1-b}} .$$

Thus equation (7) becomes

$$\frac{u}{ah} = -\left(\frac{y}{h}\right)^2 \frac{P}{2} + \frac{b}{2(2-b)P} + \frac{1-b}{2-b}\,P^{\frac{1}{1-b}} . \qquad (17)$$

Furthermore, substituting equation (13) into equation (6) we get

$$\frac{1}{a}\,\frac{\partial u}{\partial y} = -P\,\frac{y}{h} . \qquad (18)$$

Equations (17) and (18) are valid in the region $0 \leq \frac{y}{h} < \frac{1}{P}$.

Compared with the familiar parabolic velocity distribution expression for a constant viscosity liquid, equations (14) and (17) seem very complicated. However, for a special case, they become quite simple. Assume that the 1.32 percent solution of Figure C-1 is to be used. Then $b = \frac{1}{2}$ and $a = 80/\text{sec}$ and the governing equations become

$$\left.\begin{aligned} \frac{u}{ah} &= -\frac{P^2}{3}\left[\left(\frac{y}{h}\right)^3 - 1\right] \qquad (19)\\ \frac{1}{a}\,\frac{\partial u}{\partial y} &= -\left(\frac{y}{h}\right)^2 P^2 \qquad (20) \end{aligned}\right\} \quad \frac{1}{P} < \frac{y}{h} < 1$$

$$\left.\begin{aligned} \frac{u}{ah} &= -\frac{P}{2}\left(\frac{y}{h}\right)^2 + \frac{1}{6P} + \frac{P}{3}^2 \qquad (21)\\ \frac{1}{a}\,\frac{\partial u}{\partial y} &= -P\left(\frac{y}{h}\right) \qquad (22) \end{aligned}\right\} \quad 0 < \frac{y}{h} < \frac{1}{P}$$

Equations (19) and (20) pertain to the non-Newtonian region and show that the square root viscosity variation only jumps the order of the equations by one. The velocity varies as the cube of $\frac{y}{h}$, rather than the square.

Pure Newtonian flow results when P = 1, that is, when the region of $\mu = \mu_o$ = constant extends to the wall. Equations (21) and (22) apply to this case as follows:

$$\frac{u}{ah} = \frac{1}{2}\left[1 - \left(\frac{y}{h}\right)^2\right] \tag{23}$$

$$\frac{1}{a}\frac{\partial u}{\partial y} = -\frac{y}{h} \tag{24}$$

When the pressure is low enough such that only part of the Newtonian range is in use, P still equals unity but a must be replaced in equations (23) and (24) by $\left[\frac{-h}{\mu_o}\frac{dp}{dx}\right]$.

As the pressure is increased, P becomes greater than one, non-Newtonian flow appears at the wall, and part of the velocity distribution becomes cubic instead of parabolic. Figure C-3 shows the effect of P on the velocity profile, and Figure C-4 shows how $\frac{\partial u}{\partial y}$ varies with P.

The straight parts of the curves in Figure C-4 show the extent of the Newtonian region.

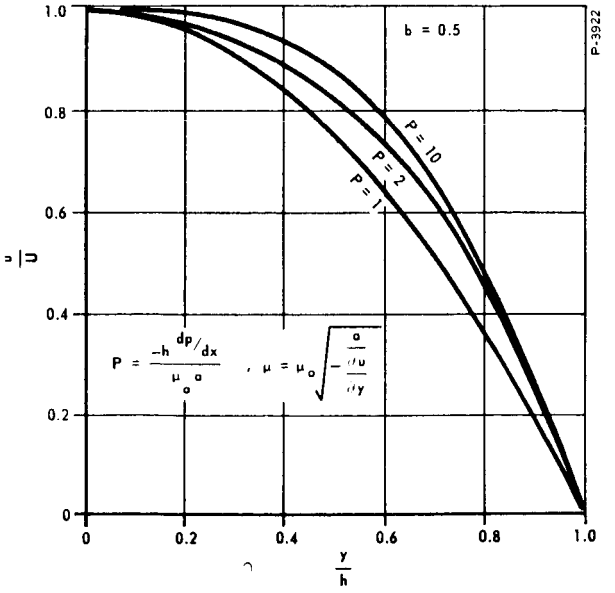

Figure C-3 - Velocity Profiles for Various Amounts of Non-Newtonian Flow

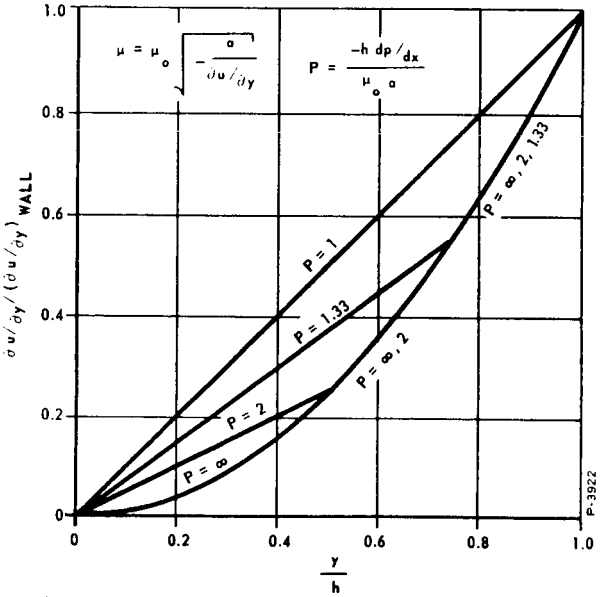

Figure C-4 - Shear Stress Distribution for Various Amounts of Non-Newtonian Flow